Chapter 2
Cold Atmospheric Pressure Plasma Sources for Cancer Applications

Mounir Laroussi, Lan Lan Nie, and XinPei Lu

Contents

Abstract In this Chapter, the physics and engineering of low-temperature plasma sources used in plasma medicine are covered. First, an overall review of the major plasma devices is presented. This is followed by a detailed description of one of the major plasma sources used in plasma oncology, the Nonequilibrium Atmospheric Pressure Plasma Jet (N-APPJ).

2.1 Review of Cold Atmospheric Pressure Plasma Sources for Cancer Applications

Cold plasmas exhibit nonequilibrium energetic conditions where the electrons have high energy while the heavy particles (ions and neutral) maintain low energy. This way, the plasma, which is weakly ionized, can have relatively low temperature, as

M. Laroussi (✉)
Plasma Engineering and Medicine Institute, Old Dominion University, Norfolk, VA, USA
e-mail: mlarouss@odu.edu

L. L. Nie · X. Lu
School of Electrical and Electronic Engineering, Huazhong University of Science and Technology, Wuhan, People's Republic of China

M. Keidar (ed.), *Plasma Cancer Therapy*, Springer Series on Atomic, Optical, and Plasma Physics 115, https://doi.org/10.1007/978-3-030-49966-2_2

low as room temperature. The main sources discussed here are the dielectric barrier discharge (DBD), the resistive barrier discharge (RBD), and the nonequilibrium atmospheric pressure plasma jets (N-APPJs). All these sources allow for the production of reactive species, such as reactive oxygen species (ROS) and reactive nitrogen species (RNS), which are believed to play key roles in the interaction of cold plasma with cells and tissues. In addition, charged species and relatively high electric fields generated by these sources can be implicated in some of the biological effects.

2.1.1 Dielectric Barrier Discharge (DBD)

History

Theodose du Moncel was the first to discover in 1855 that discharge can be generated in the gap separating two conducting plates covered by two glass plates [1]. To drive the discharge, he used a Ruhmkorff coil, which is an induction coil that allowed for the generation of high AC voltages from a low voltage DC source. This was followed, 2 years later, by the work of Werner von Siemens who reported on the application a dielectric barrier discharge (DBD) to generate ozone [2]. Siemens' design had a cylindrical geometry with tin foils as electrodes and glass as a dielectric. In the 1930s, Von Engel tried, not so successfully, to generate an atmospheric pressure nonequilibrium plasma without using a dielectric barrier, by controlling the temperature of the cathode [3]. Finally, in the late 1980s and early 1990s, reports on the generation of nonequilibrium, diffuse atmospheric pressure plasma using the DBD were published [4–6]. Planar electrode geometry and sinusoidal voltages in the kV at frequencies in the kHz range were used. The performance of the DBD was later improved when repetitive fast rise time voltage pulses with pulse widths in the nanoseconds-microseconds range were employed [7–9]. With the application of repetitive short pulses, the applied energy is preferentially coupled to the electron population and, therefore, better control of the electron energy distribution function (EEDF) is established [8–10]. DBDs have been widely used in surface-processing applications and more recently, starting around the mid-1990s, in biomedical applications, i.e., plasma medicine [11–14].

Operation of the Dielectric Barrier Discharge

The Dielectric Barrier Discharge was the first device used to generate large volume nonequilibrium atmospheric pressure diffuse plasma. Many decades of use allowed a good understanding and improvement of its operation [4–6, 15–23]. DBDs use a dielectric material, such as glass or alumina, to cover at least one of two electrodes. The electrodes are powered by high voltages (several kV) at frequencies in the kHz range. Plasma generated by DBDs can be used for surface processing, as

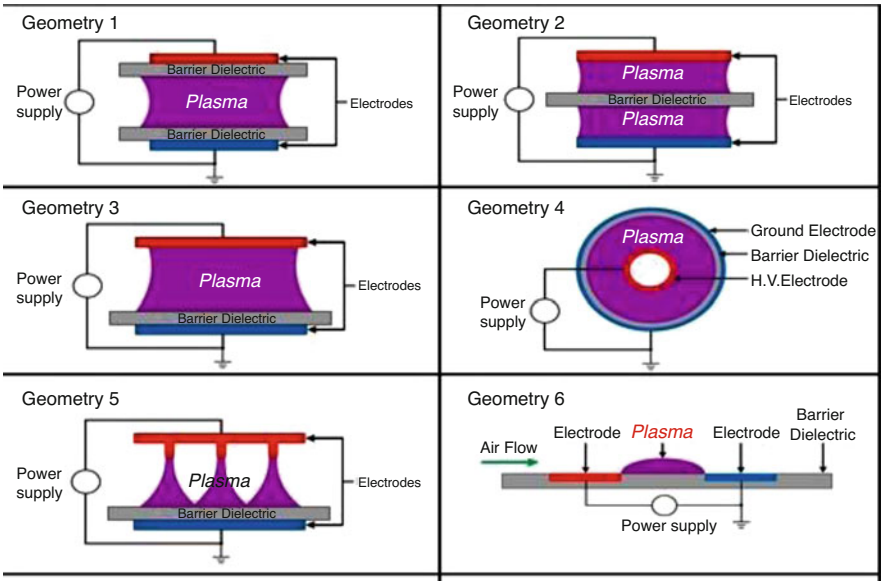

Fig. 2.1 Various DBD configurations

flow control actuators, and for the generation of ozone [16, 24, 25]. Since the mid-1990s when it was reported that cold plasma generated by DBDs inactivates bacteria efficiently, DBDs have also been used extensively for biomedical applications [11–14].

DBDs can be designed in various geometrical configurations. Figure 2.1 shows a few of them.

DBDs have been mostly energized by high sinusoidal voltages with amplitudes in the kV range and frequencies of a few kHz, or by repetitive high-voltage short pulses (ns - μs). The electrode arrangement is generally contained within a chamber to allow for the introduction of the working gas mixture. Surface charges accumulate on the dielectric surface as soon as a discharge is ignited, which creates an electrical potential that counteracts the externally applied voltage. This results in a pulsed current waveform and a self-limitation of the discharge current. Figure 2.2 shows a typical current–voltage characteristic of the DBD. Generally, DBDs produce filamentary plasmas, but under some conditions, they can produce homogeneous plasmas. Under the homogeneous operating regime, the current waveform exhibits a single pulse per half cycle, as shown in Fig. 2.2.

The electron energy distribution function (EEDF) defines/controls the chemistry in the plasma. Therefore, in order to achieve an increase of ionization and excitation, short high-voltage pulses have been used. Pulses with widths less than the characteristic time of the onset of the glow-to-arc transition maintain a stable nonequilibrium low-temperature plasma. Laroussi, Lu et al. [9] reported that two discharges occur for every applied voltage pulse. The first discharge, termed as

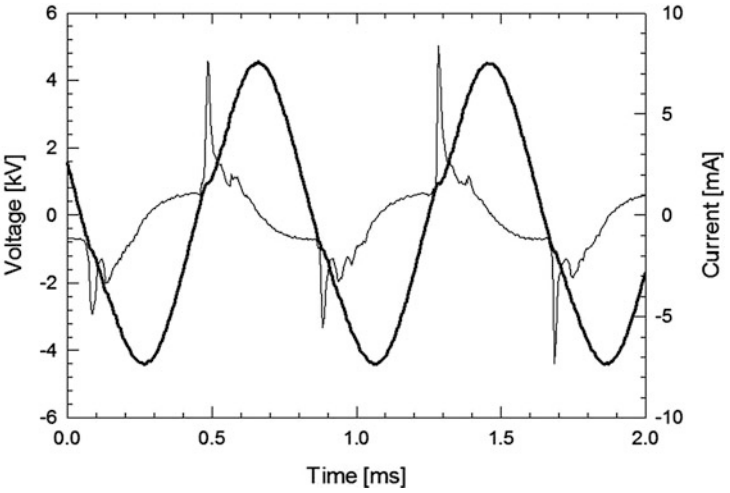

Fig. 2.2 Current–voltage characteristics of a homogeneous DBD

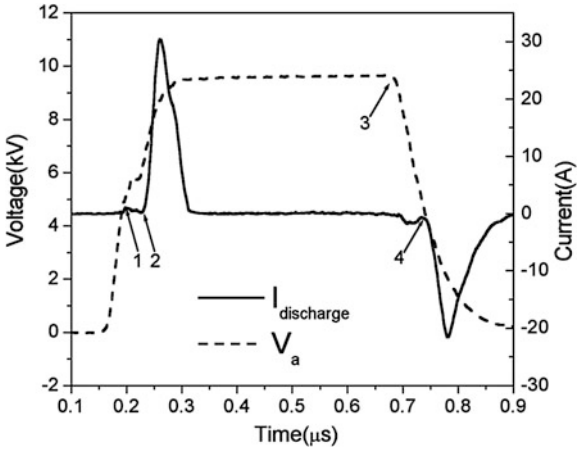

Fig. 2.3 Current–voltage characteristic of a pulsed DBD [9]

primary discharge, was ignited at the pulse rising edge while the second discharge, termed as secondary discharge, was ignited during the pulse falling edge. Figure 2.3 shows a typical current–voltage characteristic of a pulsed DBD.

2.1.2 Resistive Barrier Discharge (RBD)

DBDs require operation at frequencies in the kHz range and above. This necessitates the use of high-voltage amplifiers that can operate in this range of frequencies. To extend the operating frequency range below kHz, few methods were proposed. For

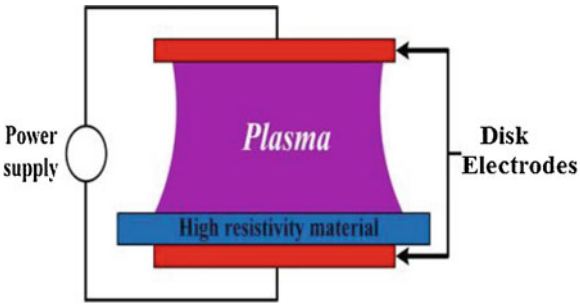

Fig. 2.4 Schematic of the resistive barrier discharge (RBD)

example, Okazaki and coworkers used a dielectric wire mesh electrode to generate a discharge at a frequency of 50 Hz [19]. Laroussi and coworkers used a high resistivity layer/film to cover one of the electrodes in a device they referred to as the Resistive Barrier Discharge (RBD) [26]. The RBD can be operated with low frequencies extending all the way to DC. The film barrier usually has a resistivity of few MΩ.cm. The high resistivity film plays the role of a distributed resistive ballast which inhibits the discharge from localizing and the current from reaching high values. This way the glow-to-arc transition is avoided. If helium is used as the operating gas a diffuse plasma can be maintained at electrodes separation gaps up to 5 cm. If a helium/air mixture is used, the plasma becomes filamentary even for small gap distances [26]. Figure 2.4 shows a schematic of the RBD.

Under both AC and DC excitation, the discharge current is a series of pulses, making the RBD a self-pulsed discharge, similar to the DBD. The pulsing of the discharge current can be explained by the combined resistive and capacitive nature of the device. When the discharge is ignited, a current starts flowing and the equivalent capacitance of the electrodes becomes charged to the point where most of the applied voltage appears across the resistive layer covering the electrodes. The voltage across the gap becomes too small to maintain a plasma. When the discharge turns off, the equivalent capacitor discharges through the resistive layer. This leads to a rapid decrease of the voltage across the resistive layer and an increase in the voltage across the gas, initiating the discharge again [27].

The RBD has been used for various industrial and biological applications including the inactivation of bacteria for sterilization/decontamination purposes [28, 29].

2.1.3 Nonequilibrium Atmospheric Pressure Plasma Jets (N-APPJs)

Nonequilibrium atmospheric pressure plasma jets (N-APPJs) are devices that can emit low-temperature plasma plumes in the surrounding air. They proved to be very useful for various plasma processing applications including biomedical applications

[14, 30, 31]. One of the attractive features of these plasma sources is the fact that they can generate a stable and controllable thin column of plasma outside the confinement of electrodes and into the surrounding environment. Because the plasma propagates away from the high-voltage region and into a region where there is no externally applied high voltage, the plasma is electrically safe and does not cause electrical shock/damage to the treated sample or exposed cells or tissues. However, the plasma plume does exhibit a very high instantaneous and local electric field at its tip. This field plays a role in the propagation of the plasma plume in the surrounding environment and can also affect the sample under treatment. Fig. 2.5 shows various designs of N-APPJs and Fig. 2.6 shows photographs of two devices, the plasma pencil and the kINPen.

The plasma plumes generated by N-APPJs are usually launched in ambient air, and as such, they provide reactive chemistry that can be exploited in biomedical applications. Reactive oxygen species (ROS), such as O, OH, O_2^-, and reactive nitrogen species (RNS), such as NO, NO_2, which can affect biological cells are produced by these devices. N-APPJs have recently been extensively used for the inactivation of pathogenic bacteria, for plasma-aided wound healing, dental applications, and the destruction of cancer cells and tumors.

The plasma plumes generated by N-APPJs are not continuous volumes of plasma but are discrete plasma packets/bullets propagating at high velocities, up to 10^5 m/s [32, 33]. Figure 2.7 shows the plasma bullets velocity as a function of time along with ICCD images of the bullets. Extensive experimental and modeling work allowed the elucidation of the mechanisms governing the generation and propagation of these plasma bullets [34–45]. Lu and Laroussi first proposed a photoionization model to explain the dynamics of the plasma bullet [33]. However, it was also shown that the high electrical field at the head of the plume plays a crucial role in the propagation process. The strength of the electric field was experimentally measured by various investigators and was found to have an average value in the 10-30 kV/cm range [46–48].

The cold plasma sources described above produce a rich "cocktail" of chemically reactive species including reactive oxygen species (ROS) and reactive nitrogen species (RNS), which are known to have important biological implication [50]. As an illustration, Figs. 2.8 and 2.9 show two important species generated by plasma jets. Figure 2.8 shows the radial distribution of hydroxyl, OH, generated by a plasma pencil for different gas flow rates. When in contact with cells the hydroxyl radical (OH) causes peroxidation of unsaturated fatty acids which are a major component of the lipids constituting the cell membrane. Fig. 2.9 shows the axial distribution of nitric oxide, NO, generated by an RF jet at different applied powers. NO has various biological effects including participation in vascular homeostasis, neurotransmission, antimicrobial defense, and immune system regulation.

Other agents generated by cold plasma sources are suspected to play active roles in biological applications. These include charges species, UV radiation, and electric fields. In fact, N-APPJs exhibit a high electric field at the tip of the plasma

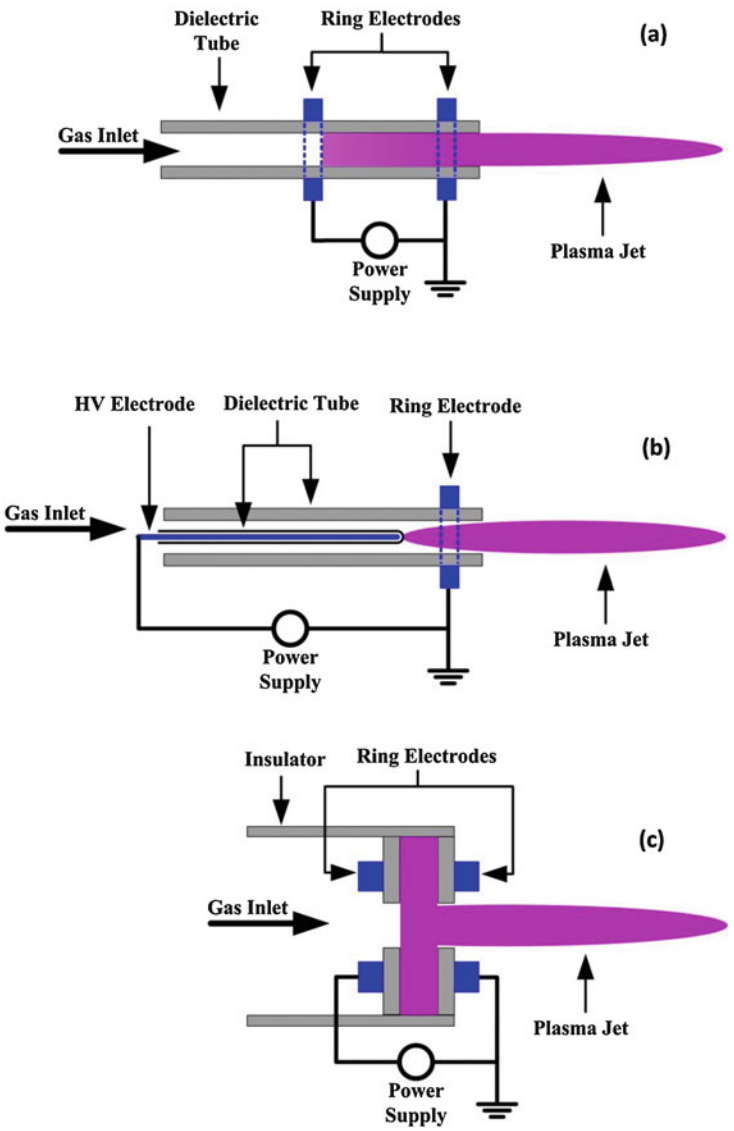

Fig. 2.5 Three different designs of N-APPJs. (**a**) Two outer ring electrodes, (**b**) An inner insulated electrode and an outer ring, (**c**) Two flat rings on perforated dielectric disks

plume. This electric field can cause electroporation of cell membranes, allowing large molecules (including ROS and RNS) to enter the cells. Figure 2.10 shows an example of the electric field generated at the head of the plume of a pulsed plasma jet as a function of axial position and pulse time.

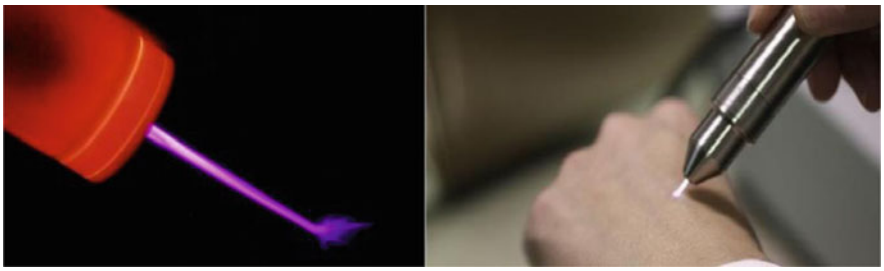

Fig. 2.6 Photos of two N-APPJs in operation: Plasma pencil (left) and the kINPen

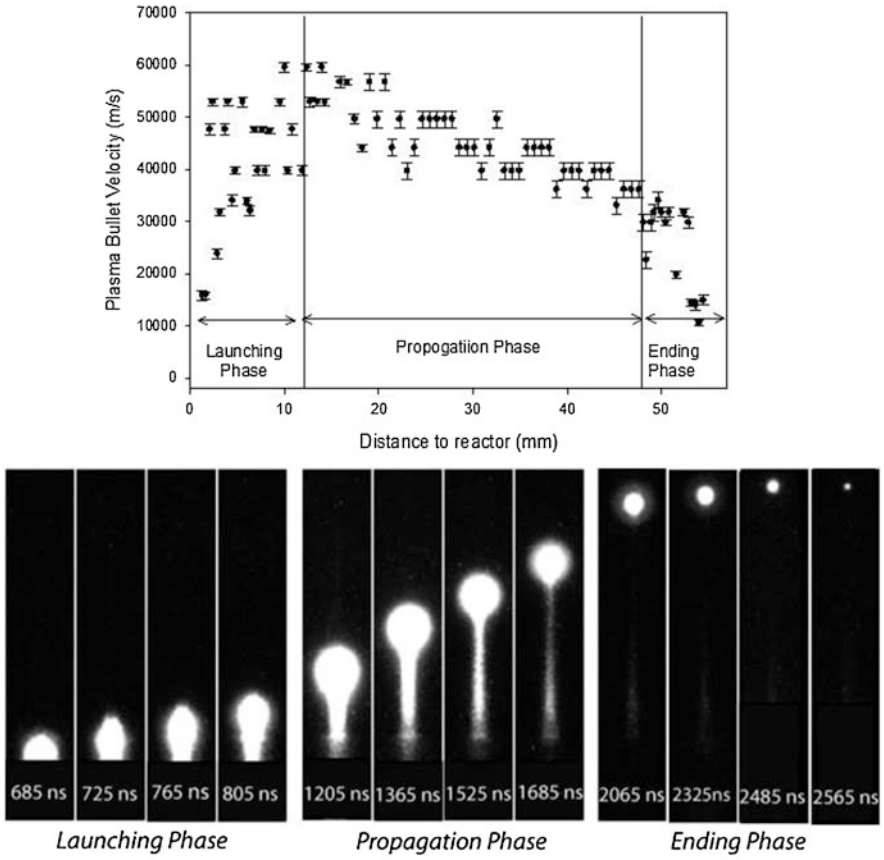

Fig. 2.7 Plasma bullet velocity as a function of distance and ICCD images [49]

Summary

Nonequilibrium atmospheric pressure plasma sources have introduced a paradigm-shifting technology in biomedicine. Early work from the mid-1990s to the early

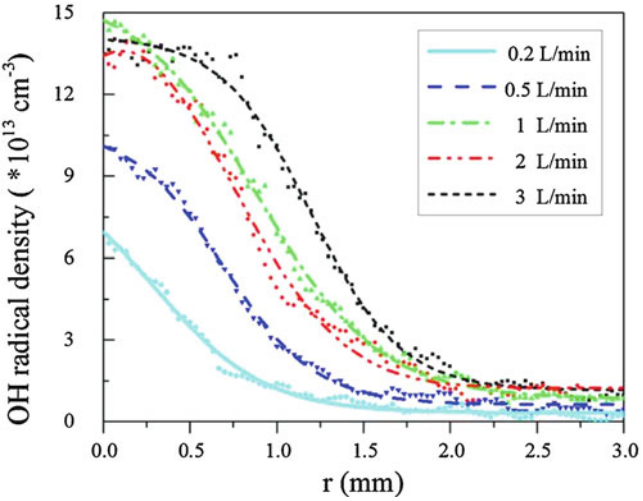

Fig. 2.8 Radial distribution of the OH density for various gas flow rates. The plasma jet (gas: helium with 115 ppm of H_2O) has an insulated single pin electrode inside a quartz tube and the plasma plume is applied on top of a water film [51]

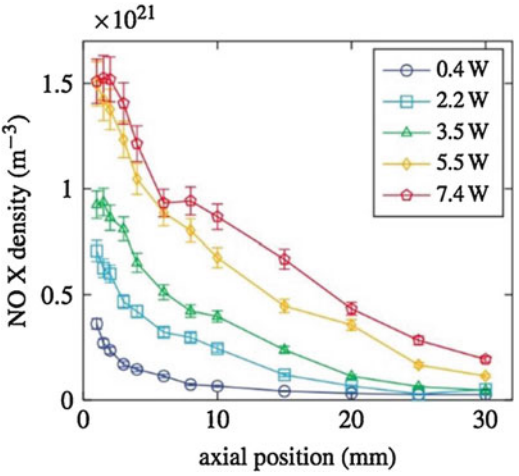

Fig. 2.9 Axial profiles of NO concentration for different discharge power. Plasma jet sustained with a RF power of 3.5 W. The plasma is operated at a frequency of 13.6 MHz, pulsed at 20 kHz with 20% duty cycle. Working gas is Ar at 1 L/min with 2% air admixture [52]

2000s showed that these cold plasma devices can be used to affect biological cells in a controlled fashion, with effects ranging from inactivation of bacteria to proliferation of fibroblasts to induction of apoptosis. These effects are mediated by the active agents generated by cold plasma, which include ROS, RNS, UV radiation, charged species, and electric fields. These agents act alone and/or synergistically. The ability to modulate biological outcomes by controlling the type and concentrations of the reactive species, the magnitude of the electric field, etc. makes cold plasma a very attractive technology upon which novel medical therapies

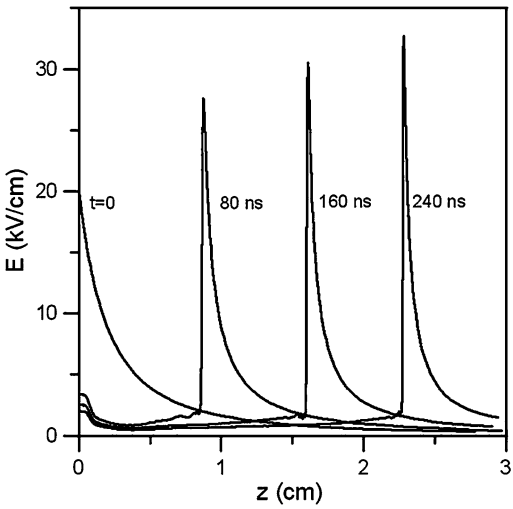

Fig. 2.10 Electric field profile of a pulsed plasma jet at various axial positions and at different times of the applied pulse [40, 53]

can be developed. Of particular interest to this book are the cancer applications. Here, investigators have shown that cold plasma can be used successfully to kill cancer cells and shrink tumors [54, 55]. Experimental in vitro and in vivo tests on numerous types of adherent and nonadherent cancer cells showed that cold plasma has the potential to be used in the treatment of some cancers either on its own or as adjuvant therapy.

2.2 Atmospheric Pressure Nonequilibrium Plasma Jets

Atmospheric pressure nonequilibrium plasma jets (APNP-Js) have received vigorous developments in recent years, which generates low-temperature plasma plume in the open air [56–61]. Without the limitation of the treatment objects, this type of gas discharge becomes the hot point for its advanced plasma chemistry, flexible structure, and pollution-free. Based on the above advantages, it has great application potential in various fields, like biomedicine [12, 62–68], material science [69–76], environment [77, 78], and so on. Normally, the plasma devices that can propagate in the open air are called APNP-Js. Another key feature of APNP-Js is its nonequilibrium, where the electron temperature is much higher than the temperature of the heavy particles. In a nonequilibrium plasma, since the electron mass is much smaller than the ion mass (less than 1/1000), the electrical energy coupled into the plasma is mainly absorbed by the electrons, so the electron temperature is significantly higher than the ion temperature [53]. The nonequilibrium of APNP-Js greatly expands its application range. For example, when the plasma jet is extremely unbalanced, the electron temperature is about 10^4 K and the gas temperature is room temperature. This nonequilibrium make the plasma is rich in reactive particles such as the OH, O, O_3, and NO which is suitable for biomedical applications [79–81].

However, there is no uniform classification standard until now, and many kinds of classification method and various names are used. For example, it can be classified by the type of working gas such as the air (or N_2, O_2) plasma jets and the noble gas plasma jets; or it can be classified by the number of the electrodes or by if there is the dielectric cover the electrode [53].

In this Section, the plasma jets are classified by the difference of the driven power and then make a more detailed division according to each category. First of all, they are divided into four parts, (1) Radio frequency driven jets; (2) Microwave power driven plasma jets; (3) AC and Pulsed DC driven plasma jets with several kilohertz; and (4) DC driven plasma jets. For the third category, the APNP-Js would been further divided into dielectric barrier discharge (DBD) jets, DBD-like jets, and floating ground electrode jets according to the presence or absence of the dielectric and the ground electrode. For the DC driven plasma jets, the APNP-Js have been classified into single electrode jets and double electrodes jets according to the number of the electrode. What's more, some work on the multi-power supply driven jets has been down, such as the AC with RF driven APNP-Js; double pulsed DC driven APNP-Js; pulsed DC with AC driven APNP-Js.

2.2.1 Radio Frequency Driven Jets

One of the early APNP-Js, developed by Hicks' group, is shown in Fig. 2.11 [82, 83]. It consists of two concentric electrodes made of stainless steel. Radio frequency power working at 13.56 MHz is applied to the inner electrode and the outer electrode is grounded. It is also named dielectric-free electrode (DFE) jets is due to its no need of a dielectric material between two electrodes [53]. Helium with oxygen or other reactive gases the mixed together and fed into the annular space between the two electrodes. Under the standard operating conditions, the RF power ranged approximately from 40 W to 500 W, and higher power leads to arcing. In order to avoid arcing, the cooling water is needed which can keep the plasma temperature at the range of 100–150 °C. Besides the cooling jacket, the stable operation condition uses greater gas flow rates such as He flow rates 25 L/min, O_2 concentrations of up to 3.0% by volume, CF_4 concentrations of up to 4.0% by volume.

This kind of DFE jet has several notable characteristics, first, the stable operation conditions must be met otherwise arcing is unavoidable. Second, the power delivered to the plasma is higher and the gas temperature is higher than the room temperature or the cell culture temperature. Third, for this DFE jet, the peak voltage is a few hundred volts and the electric field within the discharge gap is relatively low and its direction is perpendicular to the gas flow direction which means that the electric field in the plasma plume region is even lower. And the plasma plume out of the nozzle is driven by the gas flow rather than by the electrical field. On the other hand, because a relatively high power can be delivered to the plasma and the gas temperature is relatively high, the plasma is very reactive. This kind of plasma jet is suitable for applications such as material treatment as long as the material to be treated is not very sensitive to high temperatures.

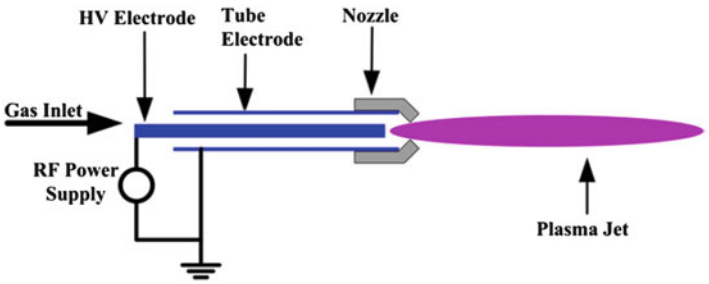

Fig. 2.11 Cross-sectional view of the RF driven APNP-Js [82]

Fig. 2.12 Photo of argon APNP-J driven by RF power supply

For the biomedical application, the plasma temperature must be lower than 40 °C and it must be safety for human touching. Many researchers have developed the RF driven plasma jets which were suitable for biomedical application [84–88]. K. D. Weltmann et al. added the dielectric between the high-voltage electrode and the ground electrode which make the discharge more stable and decrease the RF power to get lower gas temperature [89]. The commercial Argon RF device was named KINpen with different operating frequencies from 1 MHz to 40.68 MHz as shown in Fig. 2.12 The gas temperature is usually less than 40 °C. The plasma-dissipated power is approximately 1 W, with a device input power of approximately 20 W. Electron densities were expected to be up to the order of 10^{14} cm^{-3} in the streamer head at electron temperatures of up to 4 eV.

Liu et al. have obtained a 4 cm long helium cold atmospheric pressure plasma jet with pulsed radio frequency excitation as shown in Fig. 2.13 [90]. The plasma generator consisted of an 8-cm length glass tube and the same length copper electrode along the tube center. The diameter of copper electrode is 2 mm. The inner and outer diameter of the quartz tube is 5.3 mm and 8 mm. Helium fed into the tube with 5 L/min and the plasma flushed out of the generator. The pulsed RF

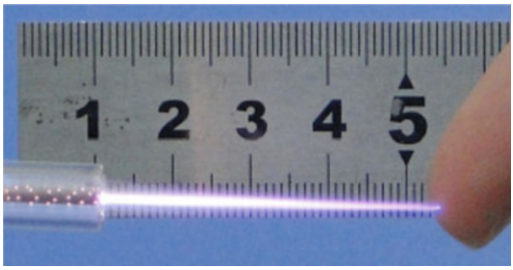

Fig. 2.13 Photo of APNP-J driven by pulsed RF power supply

voltage applied to the inner electrode with the radio frequency at 12.8 MHz and the pulsed frequency at 4 kHz. The gas temperature of the plasma plume is about the room temperature. This pulsed RF plasma jets operated at more stable state and it has overcome the easier transition to arcing.

2.2.2 Microwave Power-Driven Plasma Jets

Due to the high incident power (kW level) required to excite microwave discharge at atmospheric pressure and super-atmospheric pressure, a high-power pulse-modulated microwave source is needed for energy saving. However, it is difficult to use and control. Low-power microwave excitation and modulation of atmospheric gas discharge for a specific application is a technical problem that needs to be overcome. There have been many designs for discharge sources for microwave excitation [91–97], but the microwave power for this part of the work is mostly on the order of kW. Zhang et al. [93, 94] reported the use of a symmetric slotted antenna and the microwave discharge device realized 10 kW atmospheric pressure microwave discharge. German and Japanese researchers [95, 96] reported their experimental works of atmospheric pressure argon microwave jets which is excited by several kW power, and the periodic filament discharge characteristics of the jet have been discussed. Normally, for plasma biomedical and some temperature sensitive processing applications, the plasma temperature must be controlled, which is closely related to the microwave power.

Now, there are four typical kinds of microwave driven plasma jet devices with lower than 100 W microwave power, such as (1) coaxial transmission line resonators (CTLRs), [98, 99] (2) microstrip line resonators, [100, 101] (3) surface wave resonators [102, 103], and (4) hairpin shaped launchers [104]. There are some research studies on discharge characteristics of microwave jets. The earlier studies on CTLR operated at microwave frequencies (900 MHz and 2 GHz) were reported by Iza [105], and the devices showed great advantages such as simplicity, robustness, small ignition power, and high-power efficiency. In 2009, Choi et al. investigated the design, fabrication, and characterization of two microwave-excited microplasma sources based on coaxial transmission line resonators (CTLRs) operating at 900 MHz and 2.45 GHz [106]. In 2011, Seo et al. found that

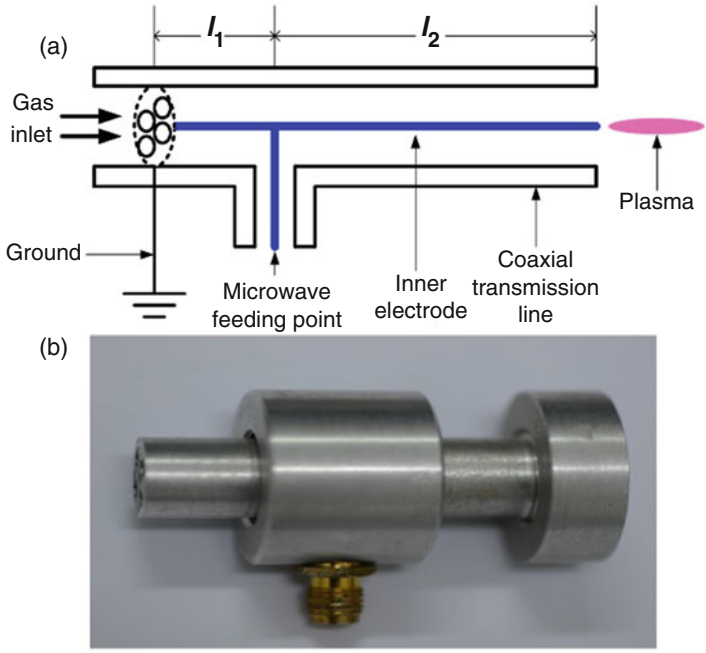

Fig. 2.14 The structure of the microwave plasma jet

microwave plasma had better electrical properties such as no electric shock for safety, high discharge current for effective chemical reactions, clean waveforms for homogenous plasma, and high power coupling efficiency by comparing two different driving frequency discharges at 13 kHz (low frequency) and 877 MHz (microwave frequency) [107]. In 2017, Chen et al. studied the argon microwave plasma jet by experiments with simulation and found that there were bullet-shaped ionization fronts ahead of this kind of plasma jet which is resonantly excited by the local enhanced electric field [108].

In 2019, Nie et al. designed a microwave plasma device with resonance frequency of 2.45 GHz [109]. The output power of the microwave source were 5 W and 10 W. The device has a short end at one side and an open end at the opposite side of the coaxial transmission line, as shown in Fig. 2.14. The diameter of the inner electrode was 1 mm, and the inner radius of the outer electrode was 4 mm. The total length of the device was approximately one-quarter of the wavelength, which was about 30 mm. The five gaseous reactive oxygen and nitrogen species (RONS) density including OH, O, O_3, NO, and NO_2 density are measured synchronously while the plasma jet is treating a biological tissue under different discharge parameters (gas composition, gas flow, skin humidity, and the output power). It has been found that the gas composition and the output power are two key factors to regulate the dose of RONS concentrations. For OH concentration, water vapor in the gas flow plays an important role. By changing the microwave power and the gas composition, the

OH concentration changes from 0.4×10^{14} cm^{-3} to 5.54×10^{14} cm^{-3}. O is mostly affected by the O_2 percentage in Ar and 1% percentage is the optimal value. O_3 is proportional to O_2 percentage in Ar and 2% O_2 can get maximum O_3 density of 6.9×10^{16} cm^{-3}. NO is in the range of 2×10^{13} cm^{-3} to 5.4×10^{14} cm^{-3} and NO_2 is in the range of 5.5×10^{14} cm^{-3} to 5×10^{15} cm^{-3}. The humidity of the skin increasing has a positive effect on the concentration of OH, O_3, and NO while a negative effect on the O and NO_2 concentrationa. For the normal skin with 40% humidity, the concentrations of the long lifetime species like O_3 and NO_2 is almost $10^{1\sim2}$ times of the other reactive species.

2.2.3 AC and Pulsed DC Driven Plasma Jets

DBD Jets

For DBD jets, as shown in Fig. 2.15a–e, there are many different configurations and all devices have a commonality, and there is dielectric layer(s) between the high-voltage electrode and the ground electrode, as shown in Fig. 2.15a, which was reported by Teschke et al. [32], the jet consists of a dielectric tube with two

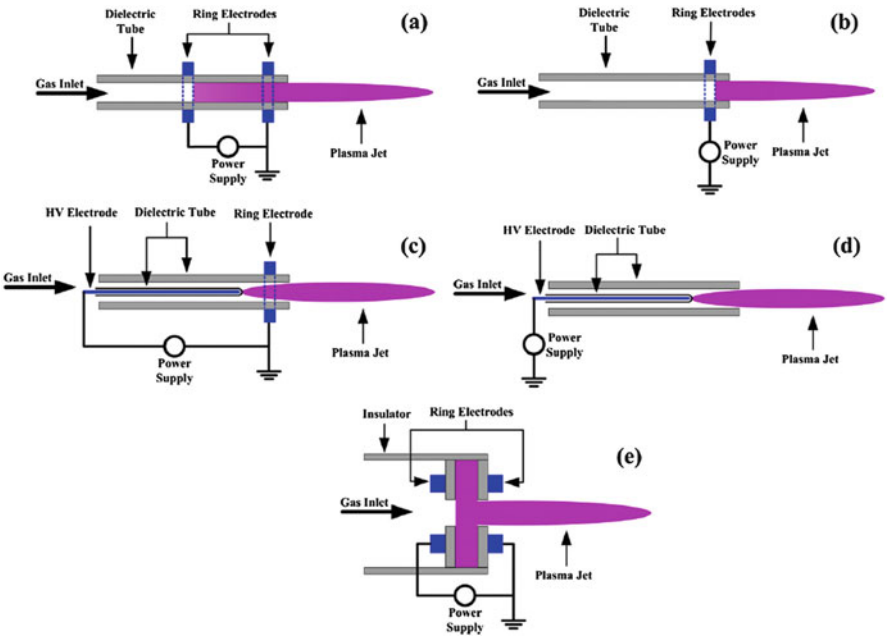

Fig. 2.15 Schematics of various DBD plasma jets. (**a**) Two outer ring electrodes, (**b**) one single outer ring electrode, (**c**) an inner insulated electrode and an outer ring, (**d**) one inner insulated electrode, (**e**) two flat rings on perforated dielectric disks

metal ring electrodes on the outer side of the tube. When a working gas (He, Ar) flows through the dielectric tube and kHz high-voltage (HV) power supply is turned on, a cold plasma jet is generated in the surrounding air. This plasma jet operation condition is easy to control with gas flow velocity less than 20 m/s. The power consumed by the plasma was only several watts, so the gas temperature is close to the room temperature. The discharge current was several mA to several tens mA which is safe for human body and cells. The plasma plume that appears homogeneous by the naked eye is actually "bullet"-like propagating along the gas flow at more than 10^4 m/s speed.

Figure 2.15b eliminates one ring electrode [110], when the jet is used acting on other objects, the objects play as the (virtual) ground electrode. Compared with two electrodes as shown in Fig. 2.12a, the discharge inside the dielectric tube is weakened. Figure 2.15c choose the pin electrode as the HV electrode and the electrode is covered by dielectric layer with one end closed [111]. With this configuration, the electric field along the plasma plume is enhanced. Walsh and Kong's studies show that a high electric field along the plasma plume is favorable for generating long plasma plumes and more active plasma chemistry [36]. Figure 2.15d further removes the ground ring electrode of Fig. 2.15c [112], so the discharge inside the tube is also weakened. On the other hand, a stronger discharge inside the discharge tube (as in the case of Fig. 2.15a and c) helps the generation of more reactive species. With the gas flow, the reactive species with relatively long lifetimes may also play an important role in various applications. The configuration of Fig. 2.15e, developed by Laroussi and Lu [31], is different from the previous four DBD jet devices. The two ring electrodes are attached to the surface of two centrally perforated dielectric disks. The holes in the center of the disks are about 3 mm in diameter. The distance between the two dielectric disks is about 5 mm. With this device, a plasma plume of up to several centimeters in length can be obtained. This plasma jet is known as the Plasma Pencil and was the earliest bio-tolerant plasma jet developed for biomedical applications.

All the DBD jet devices discussed above can be operated either by kHz ac power or by pulsed dc power. The length of the plasma jet can easily reach several centimeters or even longer than 10 cm, as reported by Lu et al. [111]. This capability makes the operation of these plasma jets easy and practical. There are several other advantages of the DBD jets. First, due to the low power density delivered to the plasma, the gas temperature of the plasma remains close to room temperature. Second, because of the use of the dielectric, there is no risk of arcing whether the object to be treated is placed far away or close to the nozzle. These two characteristics are very important for applications such as plasma medicine, where safety is a strict requirement.

DBD-Like Jets

All the plasma jet devices shown in Fig. 2.13 are named DBD-like jets. There is a dielectric layer between the HV electrode and the ground electrode, while

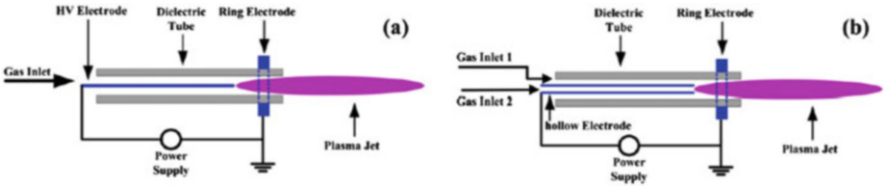

Fig. 2.16 Schematics of DBD-like plasma jets. (**a**) One inner needle electrode and one outer ring electrode, (**b**) one inner hollow tube electrode and one outer ring electrode

the plasma plume is in contact with an electrically conducting (a nondielectric material) object, especially a ground conductor, the discharge is actually running between the HV electrode and the object to be treated (ground conductor). For such a circumstance, it no longer operates as a DBD. The devices shown in Fig. 2.16 can be driven by kHz ac power, or by pulsed dc power.

Figure 2.16a the HV electrode is a bare metal needle electrode and in Fig. 2.16b, the HV electrode has been replaced by a hollow electrode [113, 114]. The main difference of two devices is that the device in Fig. 2.16b has two gas flow channel. Normally, gas inlet 1 is for a noble gas and gas inlet 2 is used for a reactive gas such as O_2 flow. It was found that the plasma plume is much longer with this kind of gas control than that using a pre-mix gas mixture with the same percentage [113]. The role (and advantage) of the ring electrode in Fig. 2.16a and b is the same as in the case of DBD jets.

When the DBD-like plasma jets are used for plasma medicine applications, the object to be treated could be cells or whole tissue. In this case, these types of jet devices should be used carefully because of the risk of arcing. On the other hand, if it is used for treatment of conductive materials, since there is no dielectric, more power can easily be delivered to the plasma. Therefore, as long as arcing is carefully avoided, the DBD-like jets have their own advantages.

Floating Electrode Jets

The floating electrode (SE) jets are shown in Fig. 2.17a–c. Figure 2.17a and b are similar to the DBD-like jets except there is no ring electrode on the outside of the dielectric tube. The dielectric tube only plays the role of guiding the gas flow.

The plasma jets shown in Fig. 2.17a and b can be driven by kHz AC and pulsed DC power. However, when they are used to work on the conductive objects, the discharge is easy to translate to arc. Considering the safety issues especially for biomedical application, the device configurations in Fig. 2.17a and b are not suitable for direct action on living organisms [115]. In order to overcome this problem, Lu et al. developed a similar SE jet, as shown in Fig. 2.17c [116]. The capacitance C and resistance R are about 50 pF and 60 kΩ, respectively. The resistor and capacitor are used for controlling the discharge current and voltage on the hollow electrode

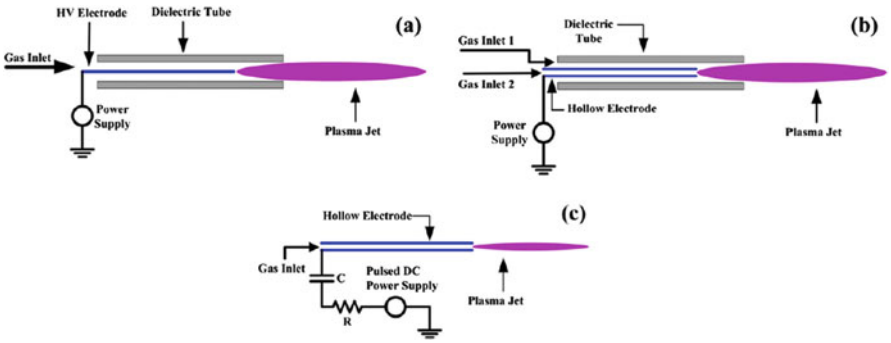

Fig. 2.17 Schematics of SE plasma jets. (**a**) One inner needle electrode, (**b**) One inner hollow tube electrode, (**c**) One hollow tube electrode without outer dielectric tubing

(needle). This jet is driven by a pulsed dc power supply with a pulse width of 500 ns, repetition frequency of 10 kHz and amplitude of 8 kV. The advantage of this jet is that the plasma plume or even the hollow electrode can be touched without any risk of injury, making it suitable for plasma medicine applications.

Based on the configuration of Fig. 2.17c, one application is the device made by Lu et al. which is used for root canal treatment [116]. Due to the narrow channel geometry of a root canal, which typically has a length of few centimeters and a diameter of 1 mm or less, the plasma generated by a plasma jet is not efficient to deliver reactive agents into the root canal for disinfection. Therefore, to have a better killing efficacy, a plasma needs to be generated inside the root canal, whereupon reactive agents, including the short-lifetime species, such as charged particles, could play some role in the killing of bacteria. As shown in Fig. 2.18, the plasma can be generated inside the root canal.

2.2.4 DC Driven Plasma Jets

Single Electrode (SE) Plasma Jets

The single-electrode plasma jets are characterized by only one high-voltage electrode, and the object to be treated acts as another electrode. The plasma is produced between the high-voltage electrode and the item being processed. In 2010, Bussiahn et al. developed a single-electrode argon APNP-J device with a negative DC drive [117]. The schematic of the device is shown in Fig. 2.19 [117]. The high-voltage electrode is a hollow needle electrode that is directly connected to a negative DC high-voltage power supply. When the input voltage is −14 kV and the volumetric flow rate is 0.5 L/min, filamentous argon APNP-J is produced in the narrow root canal. The gas temperature of argon APNP-J is 300 K. Although the input voltage is DC high voltage, the discharge current is actually in the form of a pulse with a

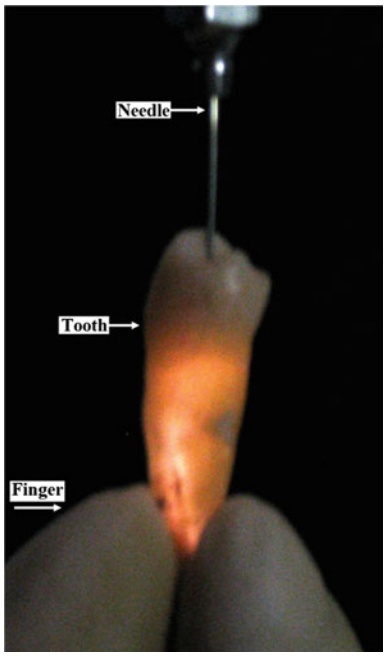

Fig. 2.18 Photograph of a plasma generated in the root canal of a tooth using the jet of Fig. 2.17c [116]

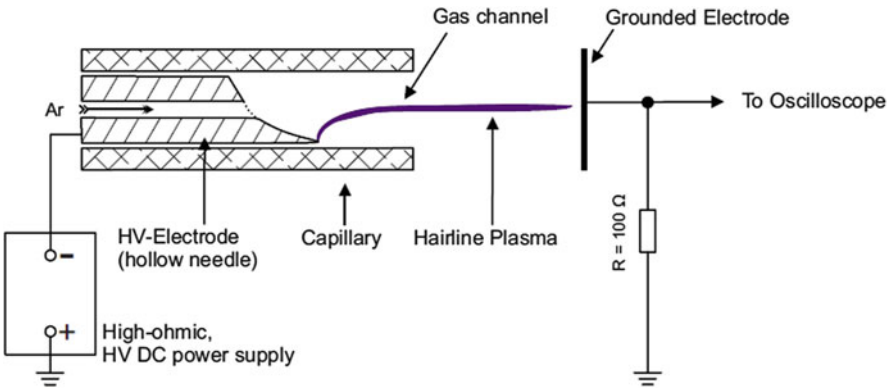

Fig. 2.19 Schematic of the hairline plasma device

pulse repetition rate of 1–3 kHz, a current peak of 1.4 A, and a pulse width of 9.8 ns. The average power consumption of argon APNP-J is 0.1 ~ 0.5 W. Bio-inactivation experiments showed that the typical pathogen Escherichia coli NTCC 10538 in the mouth was effectively inactivated by argon plasma jets.

In the same year, in order to use cheaper air as a working gas and completely remove the complicated gas supply system, Wu and Lu developed a single-electrode air APNP-J device driven by a positive DC high-voltage power supply [118]. The schematic of the device is shown in Fig. 2.20a [118]. The high-voltage electrode is

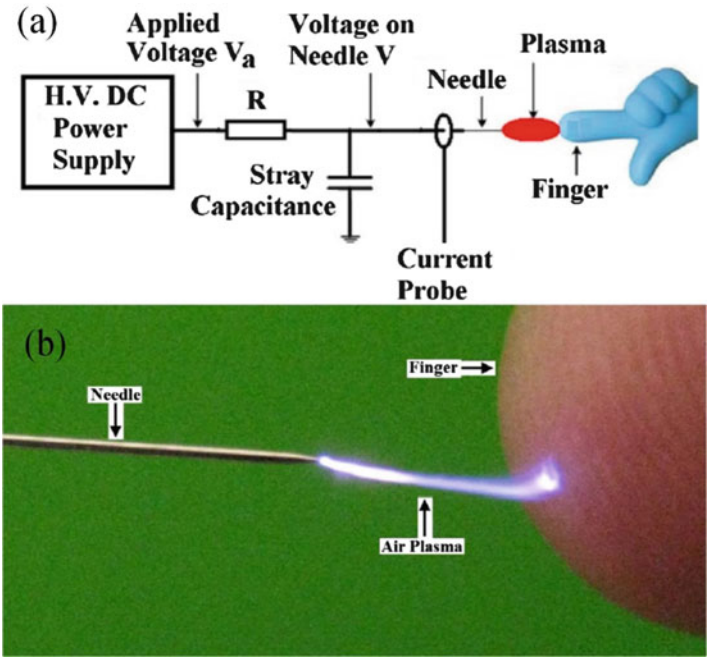

Fig. 2.20 (**a**) Schematic of air APNP-J device and (**b**) the photo of air plasma touched by a finger

a bare solid needle electrode that is connected to a high-voltage DC power supply through a large resistor with 130 MΩ resistance value. The stainless steel tip has a radius of 100 μm. The mass of the whole device is less than 1 kg. When the object to be treated is a finger, normal temperature air APNP-J can be generated between the needle tip and the finger, as shown in Fig. 2.20b [118]. The length of the air plasma plume can be up to 2 cm. The air plasma can be in safe contact with the human body without electric shock and burning sensation, and even the fingers can be safely placed on the high-voltage needle electrode. Figure 2.21 is the waveform diagram of the tip voltage and discharge current on the needle electrode (Fig. 2.21b is a partial enlarged view of Fig. 2.21a) [118]. The results show that the discharge current is actually in the form of periodic pulse. The current pulse repetition rate is approximately 25 kHz with a pulse width of 100 ns and a current peak of 17 mA. This short-pulse, low-current self-sustaining discharge mode ensures that the human body can be safely contacted. Inactivation experiments showed that the air APPJ was able to effectively inactivate Enterococcus faecalis bacteria that caused oral treatment failure.

In order to enlarge the cross section of the air APPJ, the high-voltage needle electrode was placed in a quartz tube. Figure 2.22a is the schematic diagram of the APPJ device [119]. The filament-like air APPJ section increases rapidly as the volumetric air flow rate in the tube is >1 L/min. Subsequently, an air APPJ of 0.5 cm (length) × 1 cm (width) was further successfully produced in the form of an array,

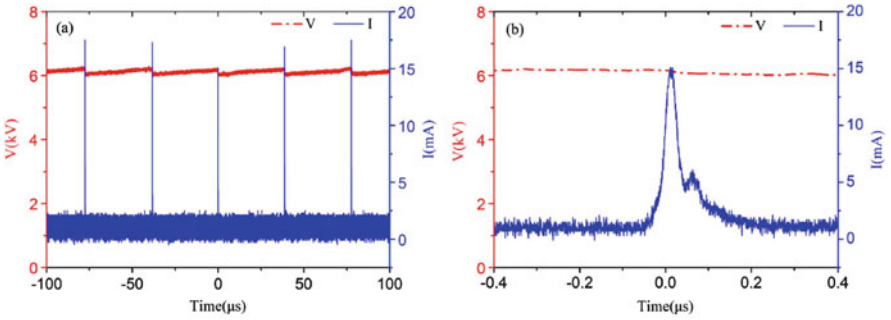

Fig. 2.21 (**a**) Current and voltage waveforms on the needle (**b**) is a partial enlarged view

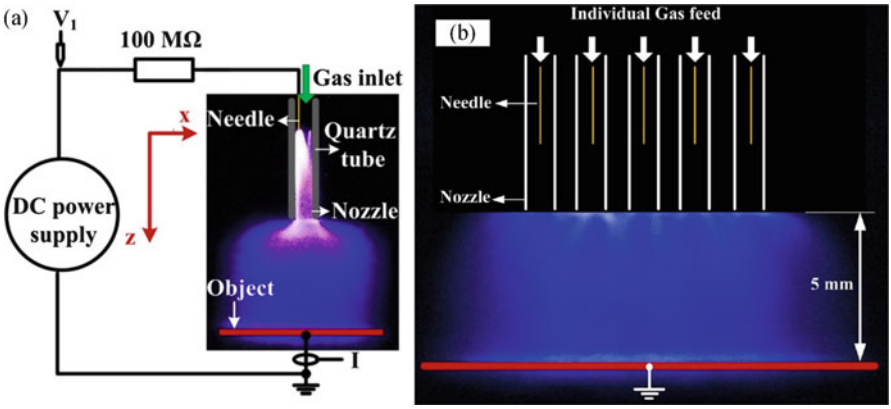

Fig. 2.22 (**a**) Schematic of air discharge device and (**b**) the photo of air plasma jet array

as shown in Fig. 2.22b [119]. It is worth noting that the air APPJ in the array overlap each other, and the spectral measurements show that the plasma radiation intensity is uniform, which is significantly different from the inert gas APPJ array [120, 121]. In this way, the quartz tube and the gas flow play an important role in increasing the cross section of the air APNP-J. Depending on the application, air APNP-Js arrays of different sizes can be arranged as desired. This is meaningful for large-area material handling and biomedical applications.

It is worth mentioning that recently, Pei and Lu developed a battery-powered, self-contained, ambient air APPJ device [122] (called plasma flashlight). Figure 2.23a is a schematic diagram of the APNP-J device [122]. The air APNP-J is driven by a 12 V battery and can be boosted to 10 kV after DC-DC conversion. The high-voltage pin electrode is connected to a high-voltage DC power supply through a current limiting resistor with a resistance of 50 MΩ. Figure 2.23b is a photo of a plasma flashlight [122]. Normal temperature air APNP-J is produced between the object to be treated and the high-voltage electrode, which is safe for touching. The device does not depend on the external power supply and the air supply circuit,

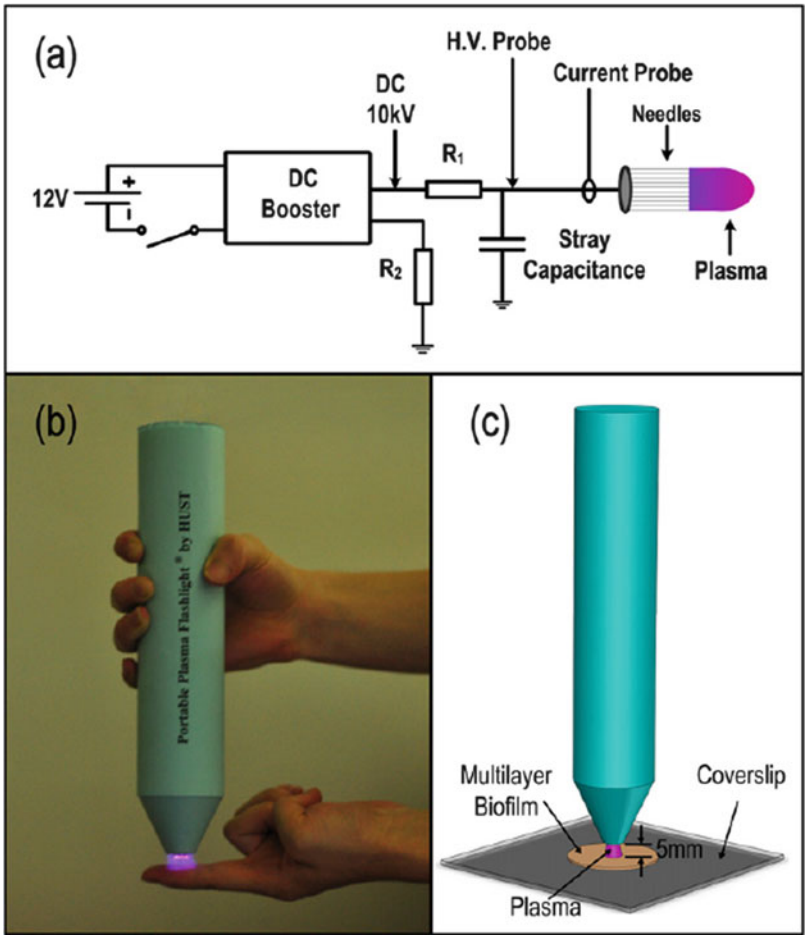

Fig. 2.23 (**a**) Schematic of the plasma jet setup, (**b**) photograph of the portable handheld plasma flashlight device, and (**c**) schematic of the biofilm treatment

making the entire experimental device small, lightweight, and highly adaptable. The experiment found that the discharge current is actually a self-pulse mode, which is similar to Fig. 2.21. The current pulse peak is about 6 mA, the pulse width is about 100 ns, the pulse repetition rate is about 20 kHz, and the power consumed on the plasma is about 60 mW. As shown in Fig. 2.23c [122], a plasma flashlight was applied to the biofilm inactivation experiment. The ambient air APNP-J was found to effectively penetrate the Enterococcus faecalis biofilm with a thickness of 25.5 μm. This portable plasma flashlight has great application prospects in the absence of AC power, such as natural disasters and wound sterilization in remote areas.

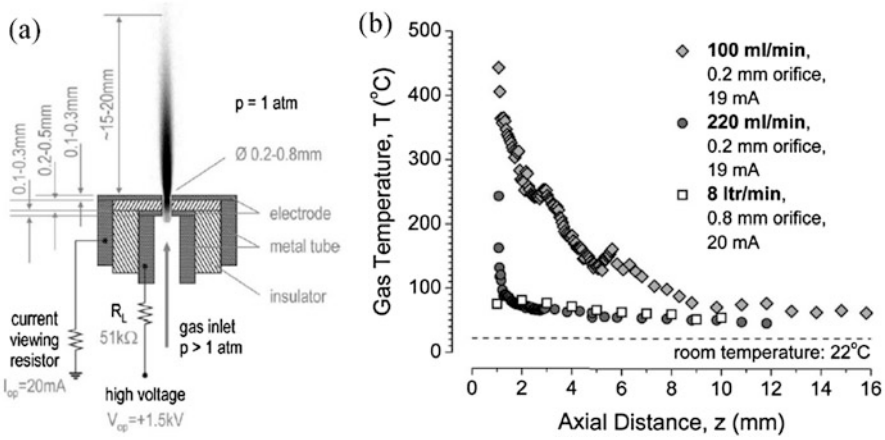

Fig. 2.24 (**a**) Schematic of air APNP-J device and (**b**) gas temperature along the plasma plume for different gas flow rate

Single-electrode air or argon APNP-Js is similar to positive corona discharge, but it is different from positive corona discharge such as the discharge current is a periodic ns pulse, the discharge mode is stable, and it is not easy to convert to glow or arc discharge.

Double Electrodes Plasma Jets

The two-electrode APNP-Js driven by a DC power source usually discharges between the high-voltage electrode and the ground electrode, and then the airflow ejects the plasma outside air. In 2008, Kolb et al. developed a two-electrode air APNP-J device [123]. The schematic of the device is shown in Fig. 2.24a [123]. The two electrodes are separated by an insulating medium with a thickness of 0.2–0.5 mm. There is a circular hole with a diameter of 0.2–0.8 mm at the center of the medium. The high-voltage electrode is connected to the high-voltage DC power supply through a 51 kΩ resistor, and the center hole on the ground electrode is the same size as the dielectric medium. When the voltage on the high-voltage electrode is 1.5–2.5 kV, gas breakdown occurs between the two electrodes to form a glow discharge, and the plasma plume injected into the air can reach a length of 1.5 cm. The temperature of the gas is determined by the velocity of the gas flow and the distance from the hole, as shown in Fig. 2.24b [123]. When the gas flow rate is 100 mL/min, the gas temperature drops from 500 °C at the nozzle to 100 °C at 1.5 cm; when the gas volume flow rate is >220 mL/min, the gas temperature outside the nozzle is close to room temperature. When the current is 20 mA, the power consumed on the plasma is about 10 W.

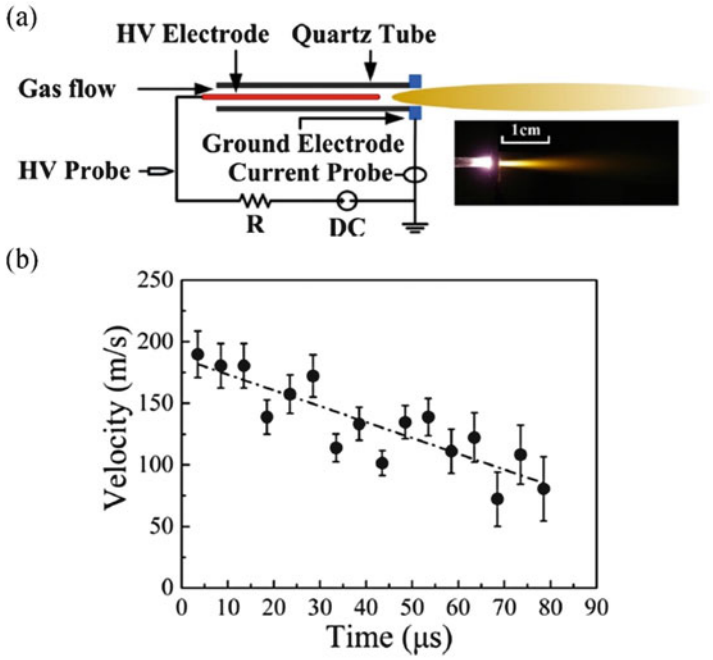

Fig. 2.25 (**a**) Schematic of discharge device and (**b**) the propagation velocity of APNP-J vs time

In addition to the glow discharge mode, Xian and Lu found that the DC-driven two-electrode nitrogen and air APNP-J also have a self-sustained pulse mode, and further studied its propulsion mechanism [124]. The APNP-J device used in the experiment is shown in Fig. 2.25a [124]. The device is similar to that developed by Kolb et al. except that the high-voltage electrode is a solid needle with a distance of 2.5 mm from ground and a current limiting resistor of 20 MΩ. Figure 2.25b shows the speed of nitrogen APNP-J with the time [124]. From the discharge dynamic process taken by the high-speed camera, it can be found that the propagation process of the two-electrode nitrogen APNP-J is similar to the "plasma bullet" propagation, but the propagation speed is not 10^4–10^5 m/s which is close to the airflow about 100 m/s. This finding demonstrates that nitrogen APNP-J is gas-driven rather than electric field driven in this two-electrode self-pulse discharge mode.

In 2013, Deng and Nikiforov et al. studied DC-driven nitrogen and air APNP-J devices [125]. The experimental setup is similar to Fig. 2.25a. Two discharge modes were also found as self-sustained pulse discharge mode and glow discharge mode. In the two discharge modes, the gas temperature of the plasma between the two electrodes is about 1000 °C, and the gas temperature of the APNP-Js outside the nozzle is close to room temperature. The air APNP-Js can generate high-density NO particles up to 1.1×10^{16} cm^{-3}.

The DC-driven single-electrode APNP-Js is similar to the DC corona discharge. The discharge has a self-pulse mode. This dissipated power is <1 W. There are two discharge modes for the DC-driven two-electrode APNP-Js: glow mode and self-pulse mode. Xian et al. have demonstrated that in self-pulsing mode, nitrogen and air APNP-Js are not driven by electric field, but are driven by airflow [124].

The DC-driven two-electrode APNP-Js consumes less than 10 W power. In general, the structural characteristics of the DC-driven APNP-Js contain two parts, one is that the high-voltage electrode is generally connected to the high-voltage DC power supply through a current limiting resistor which, is used to limit the current growth, effectively suppress the mode transition, and obtain a stable discharge mode; the other is that the higher gas flow velocity can effectively lower the gas temperature and suppress thermal instability. However, the presence of the current-limiting resistor reduces the efficiency of power supply. In single electrode air APNP-Js, the power consumed in the resistor is 0.3 W, and the power consumed on the plasma is 0.1 W [118]; in the two-electrode APNP-Js, the power consumed in the resistor is 20 W, and is consumed in The power on the plasma is <10 W [123]. Therefore, most of the power is actually consumed by the resistor, which reduces the coupling efficiency between the power source and the plasma. It is worth noting that the two-electrode APNP-Js consumes more power (which is about 10 times) than the single-electrode APNP-Js. However, due to the low cost of DC high-voltage power supply (such as battery drive), the overall power required for discharge is relatively small, the discharge structure is simple and effective, which make the handheld and portable APNP-Js be realized, so the DC-driven APNP-Js is applied. These kinds of devices are still appealing.

2.2.5 Multipower-Driven APNP-Js

AC with RF-Driven APNP-Js

In order to achieve higher activity of APNP-Js, Cao et al. used dual power supply [126]. A schematic diagram of the discharge device is shown in Fig. 2.26a [126]. The jet device consists of three electrodes, and the upstream capillary tube is inserted into the quartz tube and directly connected to the RF power source (frequency is 5.5 MHz). One ring ground electrode is wrapped at the quartz nozzle, and one plate electrode is placed downstream, and the plate electrode is connected to the AC power source with a driving frequency of 30 kHz. Figure 2.26b shows the change in APNP-J length under dual-supply interactions [126]. It is clear that the dual power supply APNP-J is longer than the single RF power drive. In addition, the experiment found that the spectral radiation intensity is stronger when the dual power supply is driven, but the gas temperature is not significantly increased. The authors believe that the plasma generated by the RF drive provides electrons for the downstream AC discharge, resulting in a higher plasma number density and

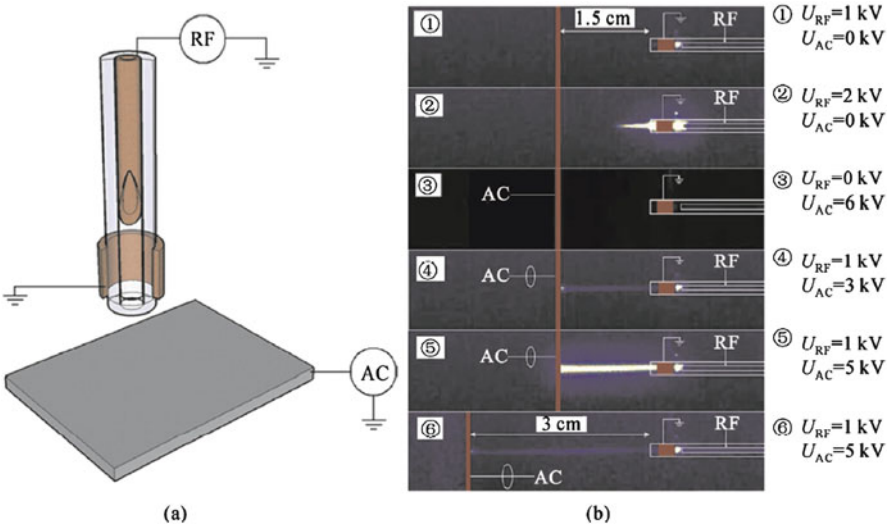

Fig. 2.26 (**a**) Schematic of discharge device driven by RF and ac power supply, and (**b**) the photo of APNP-Js (with a helium gas flow rate of 4 L/min, the distances between the tube and the grounded electrode are 1.5 cm and 3 cm, respectively)

longer plasma jet for AC discharge, while ensuring that the gas temperature is not significantly improved.

In order to further study the interaction between kHz-level AC dielectric barrier discharge and RF-driven APNP-J, Li et al. designed a special argon APNP-J device [127]. As shown in Fig. 2.27a and b [127], the APNP-J unit consists of a glass tube and 3 electrodes. The two coaxial 1 mm thick glass tubes are 2.5 mm apart which have been sealed at both ends. The two copper foils are 20 mm and 21 mm wide and are wrapped around the outer glass tube and connected to AC high voltage (frequency 50 kHz) and RF high voltage (frequency 13.56 MHz). A grounded tungsten electrode (3 mm diameter) is inserted into the inner glass tube. When the argon volume flow rate is 5 L/min and the voltages are applied, argon APNP-J can be generated in the tube. Figure 2.27c shows the voltage and current characteristics of APNP-J with or without kHz AC power supply [127]. It has been found that the kHz AC dielectric barrier discharge can effectively reduce the voltage required to produce a stable and uniform RF-driven APNP-J. By exchanging the locations of the AC and RF, a same result was obtained. This indicates that the seed electrons generated by the AC discharge are not blown by the airflow to the RF region. By adjusting the distance between the AC electrode and the RF electrode, it is found that the RF-driven uniform APNP-J can be reduced only when the distance between the two electrodes is <18 mm and the AC-driven filament discharge can reach the RF region.

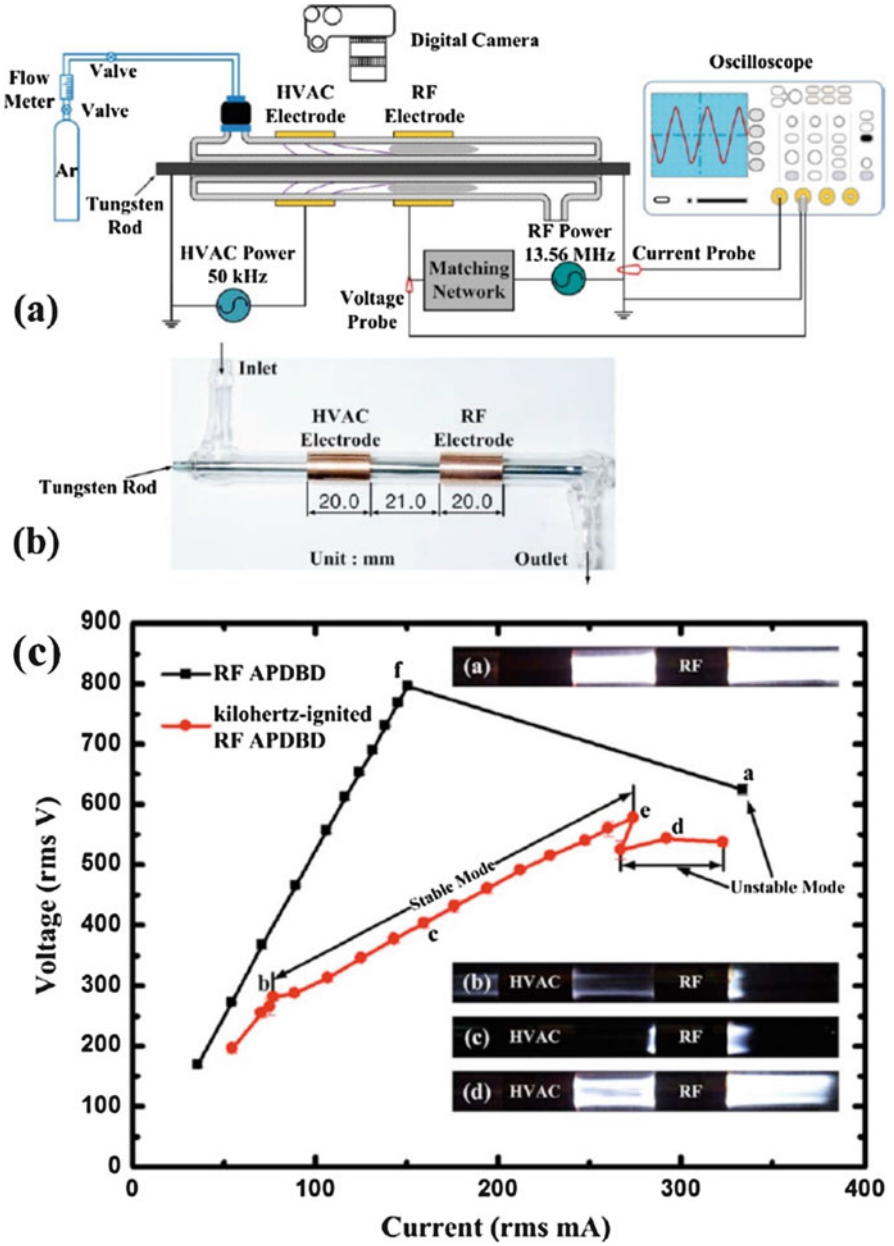

Fig. 2.27 (**a**) Schematic of discharge device, (**b**) the photo of experimental device, (**c**) and the I-V character curve driven by RF power with or without kH ac power applied (the inset images corresponds to the photos of discharge at a, b, c, and d, respectively)

Double-Pulsed DC-Driven APNP-Js

In order to more accurately control the relative change in phase and amplitude between the two power supplies, Walsh et al. used two pulsed power supplies to control the dynamic propagation of atmospheric plasma jets [128, 129]. As shown in Fig. 2.28, the main electrode structure is as follows, a copper electrode with a width of 10 mm is wrapped around a quartz tube with an inner diameter of 2 mm and a distance of 10 mm from the nozzle. The electrode is directly connected to the pulsed high-voltage power supply (the fixed pulse width is 1950 ns, with a pulse frequency of 5 kHz and an amplitude of 3.9 kV). There are two kinds of external electrode structures: one is 14 mm from the nozzle, and a ring electrode (10 mm in diameter) coaxial with the quartz tube is placed, as shown in Fig. 2.28a [128, 129]; the other is to place 2 parallel electrodes on the axis of the quartz tube which have a distance of 10 mm and a length of 60 mm as shown in Fig. 2.28b [128, 129]. The external electrodes are connected to another pulse supply (with a pulse width of 300 ns and a pulse voltage amplitude of 3 kV). When a helium gas having a volume flow rate of 3 L/min is introduced into the quartz tube and a pulse voltage is applied to the high-voltage electrode, APNP-J having a length of several cm can be produced outside the nozzle. Figure 2.28c) shows two pulse voltage and current waveform curves [128, 129].

AC and Pulsed DC Driven APNP-Js

Li et al. have studied the APNP-Js driven by AC and pulsed DC power and they have changed the phase shift between the two powers [130]. The APNP-Js structure is shown as Fig. 2.29a. The main configuration is composed of three electrodes and a clear description is given in the following. The HV electrode made of copper wire, which is connected to the ac power supply, is inserted into 4.5-cm-long quartz tube 1 with one end closed. The inner and outer diameters of quartz tube 1 are 1 and 2 mm, respectively. The ground electrode and pulsed dc ring electrode, which are attached to the outer surface of quartz tube 2, are also made of copper wire. The inner and outer diameters of quartz tube 2 are 5 and 6 mm, respectively. The HV electrode connected to ac power supply and tube 2 are aligned along tube 1. The distance between the tip of the pulsed dc ring electrode and the ground electrode is about 1 cm, while the distance between the tip of the pulsed dc ring electrode and ac HV electrode is about 0.5 cm. Figure 2.29b shows the applied voltage waveforms for both ac and pulsed dc power supplies at the phase difference of 0.

It is found that when the pulsed dc voltage is added on the negative ac half period at the phase shift of about 90°, the gas temperature reached their maximum as shown in Fig. 2.30a. On the other hand, the ground state O atom concentration has two peaks; one of the peaks also appears when the phase shift is about 90° as shown in Fig. 2.30b. When the pulsed dc voltage is applied on the positive half period at the phase shift of 270°, the O concentration reaches another peak and the peak value is higher than that when the ac or the pulsed dc power supply works alone.

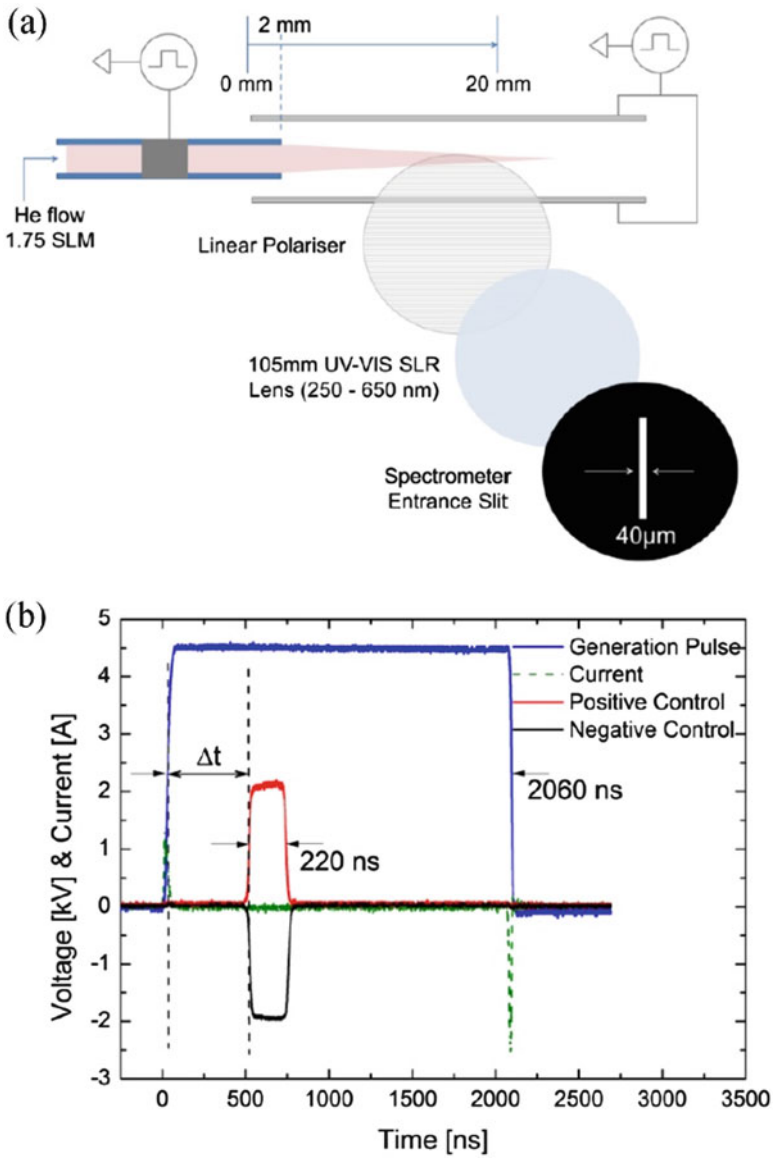

Fig. 2.28 (**a**) Schematics of discharge device with two different electrode configuration, and (**b**) current–voltage waveforms

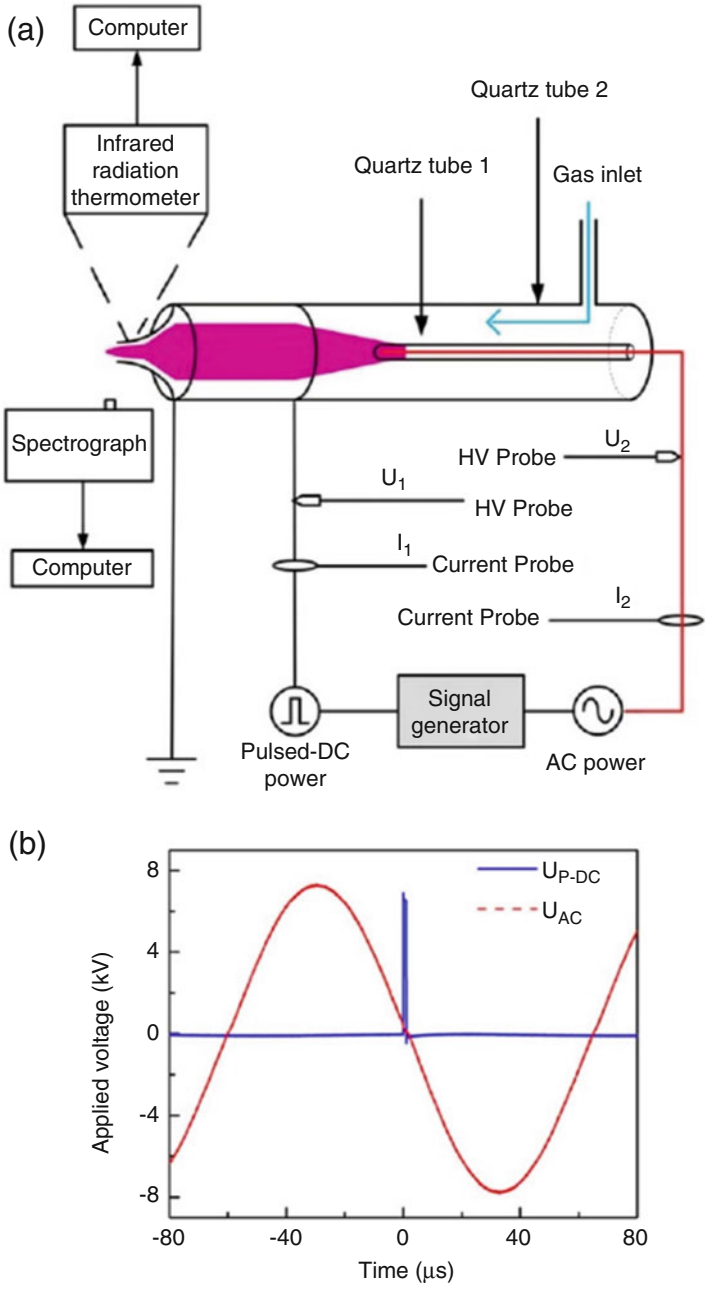

Fig. 2.29 (**a**) The schematic of the AC and pulsed DC driven APNP-Js; the phase shift between the AC voltage and pulsed DC voltage with 0° (**b**)

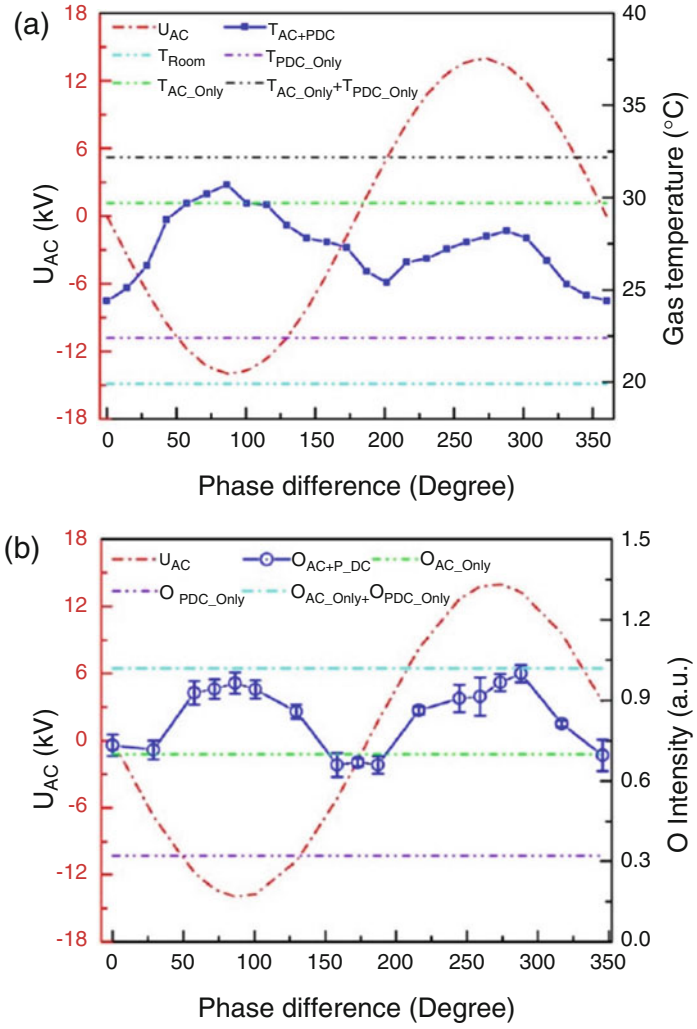

Fig. 2.30 (**a**) The gas temperature and (**b**) the O emission intensity changes with the different phase shift

References

1. Th. Du Moncel, Notice sur l'appareil d'induction electrique de Ruhmkorff et sur les experiences que l'on peut faire avec cet instrument, Hachette et Cie publishers (1855)
2. W. von Siemens, Poggendorfs. Ann. Phys. Chem. **12**, 66 (1857)
3. A. Von Engel, R. Seelinger, M. Steenbeck, Über die Glimmentladung bei hohen Drucken. Z. Phys. **85**, 144 (1933)
4. S. Kanazawa, M. Kogoma, T. Moriwaki, S. Okazaki, Stable glow at atmospheric pressure. J. Phys. D. Appl. Phys. **21**, 838 (1988)

5. F. Massines, C. Mayoux, R. Messaoudi, A. Rabehi, P. Ségur, in Experimental study of an atmospheric pressure glow discharge application to polymers surface treatment. Proc. GD-92, Swansea, UK, vol. 2 (1992), pp. 730–733
6. J.R. Roth, M. Laroussi, C. Liu, in Experimental generation of a steady-state glow discharge at atmospheric pressure. Proceedings of the IEEE International Conference on Plasma Science (1992), pp. 170–171
7. R.P. Mildren, R.J. Carman, Enhanced performance of a dielectric barrier discharge lamp using short-pulsed excitation. J. Phys. D. Appl. Phys. **34**, 3378 (2001)
8. X. Duten, D. Packan, L. Yu, C.O. Laux, C.H. Kruger, DC and pulsed glow discharges in atmospheric pressure air and nitrogen. IEEE Trans. Plasma Sci. **30**, 178 (2002)
9. M. Laroussi, X. Lu, V. Kolobov, R. Arslanbekov, Power consideration in the pulsed DBD at atmospheric pressure. J. Appl. Phys. **6**, 3028 (2004)
10. X. Lu, M. Laroussi, Temporal and spatial emission behavior of homogeneous dielectric barrier discharge driven by unipolar sub-Microsecond square pulses. J. Phys. D. Appl. Phys. **39**, 1127 (2006)
11. M. Laroussi, Sterilization of contaminated matter with an atmospheric pressure plasma. IEEE Trans. Plasma Sci. **24**, 1188 (1996)
12. M. Laroussi, Low temperature plasmas for medicine? IEEE Trans. Plasma Sci. **37**, 714 (2009)
13. G. Fridman, G. Friedman, A. Gutsol, A.B. Shekhter, V.N. Vasilets, A. Fridman, Applied plasma medicine. Plasma Process. Polym. **5**, 503 (2008)
14. K.-D. Weltmann, E. Kindel, T. von Woedtke, M. Hähnel, M. Stieber, R. Brandenburg, Atmospheric-pressure plasma sources: prospective tools for plasma medicine. Pure Appl. Chem. **82**, 1223 (2010)
15. R. Bartnikas, Note on discharges in helium under AC conditions. Br. J. Appl. Phys. (J. Phys. D.) Ser. **2**(1), 659 (1968)
16. K.G. Donohoe, The development and characterization of an atmospheric pressure nonequilibrium plasma chemical Reactor, Ph.D. thesis, California Institute of Technology, Pasadena, CA (1976)
17. T. Yokoyama, M. Kogoma, T. Moriwaki, S. Okazaki, The mechanism of the stabilized glow plasma at atmospheric pressure. J. Phys. D. Appl. Phys. **23**, 1128 (1990)
18. F. Massines, A. Rabehi, P. Decomps, R.B. Gadri, P. Ségur, C. Mayoux, Experimental and theoretical study of a glow discharge at atmospheric pressure controled by a dielectric barrier. J. Appl. Phys. **8**, 2950 (1998)
19. S. Okazaki, M. Kogoma, M. Uehara, Y. Kimura, Appearance of a stable glow discharge in air, argon, oxygen and nitrogen at atmospheric pressure using a 50 Hz source. J. Phys. D. Appl. Phys. **26**, 889 (1993)
20. N. Gherardi, G. Gouda, E. Gat, A. Ricard, F. Massines, Transition from glow silent discharge to micro-discharges in nitrogen gas. Plasma Sources Sci. Technol. **9**, 340 (2000)
21. N. Gheradi, F. Massines, Mechanisms controlling the transition from glow silent discharge to streamer discharge in nitrogen. IEEE Trans. Plasma Sci **29**, 536 (2001)
22. J.J. Shi, X.T. Deng, R. Hall, J.D. Punnett, M. Kong, Three modes in a radio frequency atmospheric pressure glow discharge. J. Appl. Phys. **94**, 6303 (2003)
23. F. Massines, N. Gherardi, N. Naude, P. Segur, Glow and Townsend dielectric barrier discharge in various atmosphere. Plasma Phys. Controlled Fusion **47**, B557 (2005)
24. U. Kogelschatz, Silent discharges for the generation of ultraviolet and vacuum ultraviolet Excimer radiation. Pure Appl. Chem. **62**, 1667 (1990)
25. U. Kogelschatz, B. Eliasson, W. Egli, Dielectric-barrier discharges: principle and applications. J. Phys. IV **7**(C4), 47 (1997)
26. M. Laroussi, I. Alexeff, J.P. Richardson, F.F. Dyer, The resistive barrier discharge. IEEE Trans. Plasma Sci **30**, 158 (2002)
27. X. Wang, C. Li, M. Lu, Y. Pu, Study on atmospheric pressure glow discharge. Plasma Sources Sci. Technol. **12**, 358 (2003)
28. M. Laroussi, J.P. Richardson, F.C. Dobbs, Effects of non-equilibrium atmospheric pressure plasmas on the heterotrophic pathways of bacteria and on their cell morphology. Appl. Phys. Lett. **81**, 772 (2002)

29. M. Laroussi, D.A. Mendis, M. Rosenberg, Plasma interaction with microbes. New J. Phys. **5**(1), 41 (2003)
30. M. Laroussi, T. Akan, Arc-free atmospheric pressure cold plasma jets: ~a review. Plasma Process. Polym. **4**, 777 (2007)
31. M. Laroussi, X. Lu, Room temperature atmospheric pressure plasma plume for biomedical applications. Appl. Phys. Lett. **87**, 113902 (2005)
32. M. Teschke, J. Kedzierski, E.G. Finantu-Dinu, D. Korzec, J. Engemann, High-speed photographs of a dielectric barrier atmospheric pressure plasma jet. IEEE Trans. Plasma Sci. **33**, 310 (2005)
33. X. Lu, M. Laroussi, Dynamics of an atmospheric pressure plasma plume generated by submicrosecond voltage pulses. J. Appl. Phys. **100**, 063302 (2006)
34. N. Mericam-Bourdet, M. Laroussi, A. Begum, E. Karakas, Experimental investigations of plasma bullets. J. Phys. D. Appl. Phys. **42**, 055207 (2009)
35. B.L. Sands, B.N. Ganguly, K. Tachibana, A streamer-like atmospheric pressure plasma jet. Appl. Phys. Lett. **92**, 151503 (2008)
36. J.L. Walsh, M.G. Kong, Contrasting characteristics of linear-field and cross-field atmospheric plasma jets. Appl. Phys. Lett. **93**, 111501 (2008)
37. Q. Xiong, X. Lu, J. Liu, Y. Xian, Z. Xiong, F. Zou, C. Zou, W. Gong, J. Hu, K. Chen, X. Pei, Z. Jiang, Y. Pan, Temporal and spatial resolved optical emission behaviors of a cold atmospheric pressure plasma jet. J. Appl. Phys. **106**, 083302 (2009)
38. E. Karakas, M. Koklu, M. Laroussi, Correlation between helium mole fraction and plasma bullet propagation in low temperature plasma jets. J. Phys. D. Appl. Phys. **43**, 155202 (2010)
39. G.V. Naidis, Modeling of plasma bullet propagation along a helium jet in ambient air. J. Phys. D. Appl. Phys. **44**, 215203 (2011)
40. G.V. Naidis, Modeling of streamer propagation in atmospheric pressure helium plasma jets. J. Phys. D. Appl. Phys. **43**, 402001 (2010)
41. M. Yousfi, O. Eichwald, N. Merbahi, N. Jomma, Analysis of ionization wave dynamics in low-temperature plasma jets from fluid modeling supported by experimental investigations. Plasma Sources Sci. Technol. **21**, 045003 (2012)
42. J.-P. Boeuf, L. Yang, L. Pitchford, Dynamics of guided streamer (plasma bullet) in a helium jet in air at atmospheric pressure. J. Phys. D. Appl. Phys. **46**, 015201 (2013)
43. E. Karakas, M. Laroussi, Experimental studies on the plasma bullet propagation and its inhibiton. J. Appl. Phys. **108**, 063305 (2010)
44. J. Jarrige, M. Laroussi, E. Karakas, Formation and dynamics of the plasma bullets in a non-thermal plasma jet: influence of the high voltage parameters on the plume characteristics. Plasma Sources Sci. Technol. **19**, 065005 (2010)
45. Y. Sakiyama, D.B. Graves, J. Jarrige, M. Laroussi, Finite elements analysis of ring-shaped emission profile in plasma bullets. Appl. Phys. Lett. **96**, 041501 (2010)
46. A. Begum, M. Laroussi, M.R. Pervez, Atmospheric pressure helium/air plasma jet: breakdown processes and propagation phenomenon. AIP Adv. **3**, 062117 (2013)
47. G.B. Stretenovic, I.B. Krstic, V.V. Kovacevic, A.M. Obradovic, M.M. Kuraica, Spatio-temporally resolved electric field measurements in helium plasma jet. J. Phys. D. Appl. Phys. **47**, 102001 (2014)
48. A. Sobota, O. Guaitella, E. Garcia-Caurel, Experimentally obtained values of electric field of an atmospheric pressure plasma jet impinging on a dielectric surface. J. Phys. D. Appl. Phys. **46**, 372001 (2013)
49. M. Laroussi, X. Lu, M. Keidar, Perspective: The physics, diagnostics, and applications of atmospheric pressure low temperature plasma sources used in plasma medicine. J. Appl. Phys. **122**, 020901 (2017)
50. X. Lu, G.V. Naidis, M. Laroussi, S. Reuter, D.B. Graves, K. Ostrikov, Reactive species in non-equilibrium atmospheric pressure plasma: generation, transport, and biological effects. Phys. Rep. **630**, 1–84 (2016)
51. Y.F. Yue, S. Mohades, M. Laroussi, X. Lu, Measurements of plasma-generated hydroxyl and hydrogen peroxide concentrations for plasma medicine applications. IEEE Trans. Plasma Sci. **44**, 2754 (2016)

52. A.F.H. van Gessel, K. Alards, P. Bruggeman, NO production in an RF plasma jet at atmospheric pressure. J. Phys. D. Appl. Phys. **46**, 265202 (2013)
53. X. Lu, M. Laroussi, V. Puech, On atmospheric pressure non-equilibrium plasma jets and plasma bullets. Plasma Sources Sci. Technol. **21**, 034005 (2012)
54. M. Laroussi, From killing bacteria to destroying cancer cells: twenty years of plasma medicine. Plasma Process. Polym. **11**, 1138 (2014)
55. M. Keidar, A. Shashurin, O. Volotskova, M.A. Stepp, P. Srinivasan, A. Sandler, B. Trink, Cold atmospheric plasma in cancer therapy. Phys. Plasmas **20**, 057101 (2013)
56. S.E. Babayan, J.Y. Jeong, A. Schutze, V.J. Tu, M. Moravej, G.S. Selwyn, R.F. Hicks, Deposition of silicon dioxide films with a nonequilibrium atmospheric-pressure plasma jet. Plasma Sources Sci. Technol. **10**, 573–578 (2001)
57. K.D. Weltmann, E. Kindel, T. von Woedtke, M. Haehnel, M. Stieber, R. Brandenburg, Atmospheric-pressure plasma sources: prospective tools for plasma medicine. Pure Appl. Chem. **82**, 1223–1237 (2010)
58. H. Ayan, E.D. Yildirim, D.D. Pappas, W. Sun, Development of a cold atmospheric pressure microplasma jet for freeform cell printing. Appl. Phys. Lett. **99**(11), 111502 (2011)
59. J.J. Lowke, Plasma predictions: past, present and future. Plasma Sources Sci. Technol. **22**(2), 023002 (2013)
60. S. Samukawa, M. Hori, S. Rauf, K. Tachibana, P. Bruggeman, G. Kroesen, J.C. Whitehead, A.B. Murphy, A.F. Gutsol, S. Starikovskaia, U. Kortshagen, J.-P. Boeuf, T.J. Sommerer, M.J. Kushner, U. Czarnetzki, N. Mason, The 2012 plasma roadmap. J. Phys. D. Appl. Phys. **45**(25), 253001 (2012)
61. M. Laroussi, Low temperature plasma-based sterilization: overview and state-of-the-art. Plasma Process. Polym. **2**, 391–400 (2005)
62. G. Fridman, A. Gutsol, A.B. Shekhter, V.N. Vasilets, A. Fridman, Applied plasma medicine. Plasma Process. Polym. **5**, 503–533 (2008)
63. R. Diwan, F.M. Debta, A. Deoghare, S. Ghom, A. Khandelwal, S.D. Sikdar, A.G. Ghom, Plasma therapy: an overview. J. Indian Acad. Oral Med. Radiol. **23**, 120–123 (2011)
64. T. von Woedtke, S. Reuter, K. Masur, K.D. Weltmann, Plasmas for medicine. Phys. Rep. **530**, 291–320 (2013)
65. M.G. Kong, G. Kroesen, G. Morfill, T. Nosenko, T. Shimizu, J. van Dijk, J.L. Zimmermann, Plasma medicine: an introductory review. New J. Phys. **11**, 115012 (2009)
66. G.E. Morfill, M.G. Kong, J.L. Zimmermann, Focus on plasma medicine. New J. Phys. **11**, 115011 (2009)
67. E.C. Neyts, M. Yusupov, C.C. Verlackt, A. Bogaerts, Computer simulations of plasma-biomolecule and plasma-tissue interactions for a better insight in plasma medicine. J. Phys. D. Appl. Phys. **47**(29), 293001 (2014)
68. X. Lu, Guest editorial: atmospheric pressure plasma jets and their applications. IEEE Trans. Plasma Sci. **43**, 701–702 (2015)
69. K. Fricke, H. Steffen, T. von Woedtke, K. Schroeder, K.-D. Weltmann, High rate etching of polymers by means of an atmospheric pressure plasma jet. Plasma Process. Polym. **8**, 51–58 (2011)
70. T.-C. Tsai, D. Staack, Low-temperature polymer deposition in ambient air using a floating-electrode dielectric barrier discharge jet. Plasma Process. Polym. **8**, 523–534 (2011)
71. D. Wang, Q. Yang, Y. Guo, X. Liu, J. Shi, J. Zhang, One step growth of TiO2 crystal trees by atmospheric pressure plasma jet. Mater. Lett. **65**, 2526–2529 (2011)
72. K. Kelly-Wintenberg, T.C. Montie, C. Brickman, J.R. Roth, A.K. Carr, K. Sorge, et al., Room temperature sterilization of surfaces and fabrics with a one atmosphere uniform glow discharge plasma. J. Ind. Microbiol. Biotechnol. **20**, 69–74 (1998)
73. O. Sakai, K. Tachibana, Plasmas as metamaterials: a review. Plasma Sources Sci. Technol. **21**(1), 013001 (2012)
74. K. Ostrikov, Colloquium: Reactive plasmas as a versatile nanofabrication tool. Rev. Mod. Phys. **77**, 489–511 (2005)

75. D. Kolacyak, J. Ihde, C. Merten, A. Hartwig, U. Lommatzsch, Fast functionalization of multi-walled carbon nanotubes by an atmospheric pressure plasma jet. J. Colloid Interface Sci. **359**, 311–317 (2011)
76. K. Ostrikov, E.C. Neyts, M. Meyyappan, Plasma nanoscience: from nano-solids in plasmas to nano-plasmas in solids. Adv. Phys. **62**, 113–224 (2013)
77. P. Bruggeman, J. Liu, J. Degroote, M.G. Kong, J. Vierendeels, C. Leys, Dc excited glow discharges in atmospheric pressure air in pin-to-water electrode systems. J. Phys. D. Appl. Phys. **41**, 215201 (2008)
78. P. Bruggeman, C. Leys, Non-thermal plasmas in and in contact with liquids. J. Phys. D. Appl. Phys. **42**, 053001 (2009)
79. X. Lu, S. Wu, On the active species concentrations of atmospheric pressure nonequilibrium plasma jets. IEEE Trans. Plasma Sci. **41**, 2313–2326 (2013)
80. G. Fridman, A.D. Brooks, M. Balasubramanian, A. Fridman, A. Gutsol, V.N. Vasilets, H. Ayan, G. Friedman, Comparison of direct and indirect effects of non-thermal atmospheric-pressure plasma on bacteria. Plasma Process. Polym. **4**, 370–375 (2007)
81. J.Y. Kim, Y. Wei, J. Li, S.-O. Kim, 15 um-sized single-cellular-level and cell-manipulatable microplasma jet in cancer therapies. Biosens. Bioelectron. **26**, 555–559 (2010)
82. S.E. Babayan, J.Y. Jeong, V.J. Tu, J. Park, G.S. Selwyn, R.F. Hicks, Deposition of silicon dioxide films with an atmospheric-pressure plasma jet. Plasma Sources Sci. Technol. **7**, 286–288 (1998)
83. J.Y. Jeong, S.E. Babayan, V.J. Tu, J. Park, I. Henins, R.F. Hicks, G.S. Selwyn, Etching materials with an atmospheric-pressure plasma jet. Plasma Sources Sci. Technol. **7**, 282–285 (1998)
84. J.-Y. Choi, N. Takano, K. Urabe, K. Tachibana, Measurement of electron density in atmospheric pressure small-scale plasmas using CO2-laser heterodyne interferometry. Plasma Sources Sci. Technol. **18**(3), 035013 (2009)
85. S.C. Snyder, D.M. Crawford, J.R. Fincke, Dependence on the scattering angle of the electron temperature and electron density in Thomson-scattering measurements on an atmospheric-pressure plasma jet (vol 61, pg 1920, 2000). Phys. Rev. E **61**, 7261–7261 (2000)
86. S.-Z. Li, D.-Z. Wang, W.-C. Zhu, Y.-K. Pu, Evaluations of electron density and temperature in atmospheric-pressure radio-frequency helium plasma jet. Jpn. J. Appl. Phys. Part 1 **45**, 9213–9215 (2006)
87. S. Hofmann, A.F.H. van Gessel, T. Verreycken, P. Bruggeman, Power dissipation, gas temperatures and electron densities of cold atmospheric pressure helium and argon RF plasma jets (vol 20, 065010, 2011). Plasma Sources Sci. Technol. **21**(6), 069501 (2012)
88. M. Qian, C. Ren, D. Wang, J. Zhang, G. Wei, Stark broadening measurement of the electron density in an atmospheric pressure argon plasma jet with double-power electrodes. J. Appl. Phys. **107**(6), 063303 (2010)
89. K.D. Weltmann, R. Brandenburg, T. von Woedtke, J. Ehlbeck, R. Foest, M. Stieber, E. Kindel, Antimicrobial treatment of heat sensitive products by miniaturized atmospheric pressure plasma jets (APPJs). J. Phys. D. Appl. Phys. **41**, 194008 (2008)
90. J.H. Liu, X.Y. Liu, K. Hu, D.W. Liu, X.P. Lu, F. Iza, M.G. Kong, Plasma plume propagation characteristics of pulsed radio frequency plasma jet. Appl. Phys. Lett. **98**, 151502 (2011)
91. Y. Hidaka, E.M. Choi, I. Mastovsky, M.A. Shapiro, J.R. Sirigiri, R.J. Temkin, Observation of large arrays of plasma filaments in air breakdown by 1.5-MW 110-GHz gyrotron pulses. Phys. Rev. Lett. **100**, 035003 (2008)
92. K.V. Aleksandrov, V.L. Bychkov, I.I. Esakov, L.P. Grachev, K.V. Khodataev, A.A. Ravaev, I.B. Matveev, Investigations of subcritical streamer microwave discharge in reverse-vortex combustion chamber. IEEE Trans. Plasma Sci. **37**, 2293–2297 (2009)
93. Q. Zhang, G. Zhang, L. Wang, X. Wang, S. Wang, Y. Chen, Measurement of the electron density in a microwave plasma torch at atmospheric pressure. Appl. Phys. Lett. **95**, 201502 (2009)
94. Z. Wang, G. Zhang, Q. Zhang, Z. Jia, A large-volume open-air microwave plasma based on parallel multislot rectangular waveguides. IEEE Trans. Plasma Sci. **40**, 1380–1385 (2012)

95. J. Hnilica, V. Kudrle, P. Vasina, J. Schaefer, V. Aubrecht, Characterization of a periodic instability in filamentary surface wave discharge at atmospheric pressure in argon. J. Phys. D. Appl. Phys. **45**, 055201 (2012)
96. S. Takamura, S. Amano, T. Kurata, H. Kasada, J. Yamamoto, M.A. Razzak, G. Kushida, N. Ohno, M. Kando, Formation and decay processes of Ar/He microwave plasma jet at atmospheric gas pressure. J. Appl. Phys. **110**, 043301 (2011)
97. Q. Wang, L. Hou, G. Zhang, B. Zhang, C. Liu, Z. Wang, J. Huang, Using indium tin oxide material to implement the imaging of microwave plasma ignition process. Appl. Phys. Lett. **104**, 074107 (2014)
98. Z. Chen, Z. Yin, M. Chen, L. Hong, G. Xia, Y. Hu, Y. Huang, M. Liu, A.A. Kudryavtsev, Self-consistent fluid modeling and simulation on a pulsed microwave atmospheric-pressure argon plasma jet. J. Appl. Phys. **116**, 153303 (2014)
99. H.W. Lee, S.K. Kang, I.H. Won, H.Y. Kim, H.C. Kwon, J.Y. Sim, J.K. Lee, Distinctive plume formation in atmospheric Ar and He plasmas in microwave frequency band and suitability for biomedical applications. Phys. Plasmas **20**, 123506 (2013)
100. C. Wu, A.R. Hoskinson, J. Hopwood, Stable linear plasma arrays at atmospheric pressure. Plasma Sources Sci. Technol. **20**, 045022 (2011)
101. A.R. Hoskinson, J. Hopwood, A two-dimensional array of microplasmas generated using microwave resonators. Plasma Sources Sci. Technol. **21**, 052002 (2012)
102. E. Carbone, N. Sadeghi, E. Vos, S. Hubner, E. van Veldhuizen, J. van Dijk, S. Nijdam, G. Kroesen, Spatio-temporal dynamics of a pulsed microwave argon plasma: ignition and afterglow. Plasma Sources Sci. Technol. **24**, 015015 (2015)
103. E.A.D. Carbone, S. Huebner, J.M. Palomares, J.J.A.M. van der Mullen, The radial contraction of argon microwave plasmas studied by Thomson scattering. J. Phys. D. Appl. Phys. **45**, 345203 (2012)
104. Z. Chen, G. Xia, C. Zou, P. Li, Y. Hu, Q. Ye, S. Eliseev, O. Stepanova, A.I. Saifutdinov, A.A. Kudryavtsev, M. Liu, Study on hairpin-shaped argon plasma jets resonantly excited by microwave pulses at atmospheric pressure. J. Appl. Phys. **118**, 023307 (2015)
105. F. Iza, J.A. Hopwood, Low-power microwave plasma source based on a microstrip split-ring resonator. IEEE Trans. Plasma Sci. **31**, 782 (2003)
106. J. Choi, F. Iza, H.J. Do, J.K. Lee, M.H. Cho, Microwave-excited atmospheric-pressure microplasmas based on a coaxial transmission line resonator. Plasma Sources Sci. Technol. **18**, 025029 (2009)
107. Y.S. Seo, H.W. Lee, H.C. Kwon, J. Choi, S.M. Lee, K.C. Woo, K.T. Kim, J.K. Lee, A study on characterization of atmospheric pressure plasma jets according to the driving frequency for biomedical applications. Thin Solid Films **519**, 7071–7078 (2011)
108. Z. Chen, G. Xia, C. Zou, X. Liu, D. Feng, P. Li, Y. Hu, O. Stepanova, A.A. Kudryavtsev, Bullet-shaped ionization front of plasma jet plumes driven by microwave pulses at atmospheric gas pressure. J. Appl. Phys. **122**, 093301 (2017)
109. J. Zhao, L. Nie, Five gaseous reactive oxygen and nitrogen species (RONS) density generated by microwave plasma jet. Phys. Plasmas **26**, 073503 (2019)
110. Q. Li, J.-T. Li, W.-C. Zhu, X.-M. Zhu, Y.-K. Pu, Effects of gas flow rate on the length of atmospheric pressure nonequilibrium plasma jets. Appl. Phys. Lett. **95**, 141502 (2009)
111. X. Lu, Z. Jiang, Q. Xiong, Z. Tang, X. Hu, Y. Pan, An 11 cm long atmospheric pressure cold plasma plume for applications of plasma medicine. Appl. Phys. Lett. **92**, 081502 (2008)
112. X. Lu, Z. Jiang, Q. Xiong, Z. Tang, Y. Pan, A single electrode room-temperature plasma jet device for biomedical applications. Appl. Phys. Lett. **92**, 151504 (2008)
113. V. Leveille, S. Coulombe, Design and preliminary characterization of a miniature pulsed RF APGD torch with downstream injection of the source of reactive species. Plasma Sources Sci. Technol. **14**, 467–476 (2005)
114. A. Shashurin, M.N. Shneider, A. Dogariu, R.B. Miles, M. Keidar, Temporal behavior of cold atmospheric plasma jet. Appl. Phys. Lett. **94**, 231504 (2009)
115. E. Stoffels, I.E. Kieft, R.E.J. Sladek, Superficial treatment of mammalian cells using plasma needle. J. Phys. D. Appl. Phys. **36**, 2908–2913 (2003)

116. X. Lu, Y.G. Cao, P. Yang, Q. Xiong, Z.L. Xiong, Y.B. Xian, Y. Pan, An RC plasma device for sterilization of root canal of teeth. IEEE Trans. Plasma Sci. **37**, 668–673 (2009)
117. R. Bussiahn, R. Brandenburg, T. Gerling, E. Kindel, H. Lange, N. Lembke, K.D. Weltmann, T. von Woedtke, T. Kocher, The hairline plasma: an intermittent negative dc-corona discharge at atmospheric pressure for plasma medical applications. Appl. Phys. Lett. **96**, 143701 (2010)
118. S. Wu, X. Lu, Z. Xiong, Y. Pan, A touchable pulsed air plasma plume driven by DC power supply. IEEE Trans. Plasma Sci. **38**, 3404–3408 (2010)
119. S. Wu, Z. Wang, Q. Huang, X. Lu, K. Ostrikov, Open-air direct current plasma jet: scaling up, uniformity, and cellular control. Phys. Plasmas **19**, 103503 (2012)
120. Z. Cao, J.L. Walsh, M.G. Kong, Atmospheric plasma jet array in parallel electric and gas flow fields for three-dimensional surface treatment. Appl. Phys. Lett. **94**, 21501 (2009)
121. X. Pei, Z. Wang, Q. Huang, S. Wu, X. Lu, Dynamics of a plasma jet Array. IEEE Trans. Plasma Sci. **39**, 2276–2277 (2011)
122. X. Pei, X. Lu, J. Liu, D. Liu, Y. Yang, K. Ostrikov, P.K. Chu, Y. Pan, Inactivation of a 25.5 um Enterococcus faecalis biofilm by a room-temperature, battery-operated, handheld air plasma jet. J. Phys. D. Appl. Phys. **45**(16), 165205 (2012)
123. J.F. Kolb, A.A.H. Mohamed, R.O. Price, R.J. Swanson, A. Bowman, R.L. Chiavarini, M. Stacey, K.H. Schoenbach, Cold atmospheric pressure air plasma jet for medical applications. Appl. Phys. Lett. **92**, 241501 (2008)
124. Y. Xian, X. Lu, S. Wu, P.K. Chu, Y. Pan, Are all atmospheric pressure cold plasma jets electrically driven? Appl. Phys. Lett. **100**, 123702 (2012)
125. X.L. Deng, A.Y. Nikiforov, P. Vanraes, C. Leys, Direct current plasma jet at atmospheric pressure operating in nitrogen and air. J. Appl. Phys. **113**, 23305 (2013)
126. Z. Cao, Q.Y. Nie, M.G. Kong, A cold atmospheric pressure plasma jet controlled with spatially separated dual-frequency excitations. J. Phys. D. Appl. Phys. **42**, 222003 (2009)
127. P.-S. Le, G. Li, S. Wang, H.-P. Li, C.-Y. Bao, Characteristics of kilohertz-ignited, radio-frequency atmospheric-pressure dielectric barrier discharges in argon. Appl. Phys. Lett. **95**(20), 201501 (2009)
128. P. Olszewski, E. Wagenaars, K. McKay, J.W. Bradley, J.L. Walsh, Measurement and control of the streamer head electric field in an atmospheric-pressure dielectric barrier plasma jet. Plasma Sources Sci. Technol. **23**, 015010 (2014)
129. G.V. Naidis, J.L. Walsh, The effects of an external electric field on the dynamics of cold plasma jets-experimental and computational studies. J. Phys. D. Appl. Phys. **46**(9), 095203 (2013)
130. J. Li, F. Wu, L. Nie, X. Lu, The effect of phase shift on the plasma driven by an AC voltage and a pulsed DC voltage. IEEE Trans. Plasma Sci. **47**, 1–9 (2019)